INL/EXT-13-29727

Characterization of Radiolytically Generated Degradation Products in the Strip Section of a TRUEX Flowsheet

Dean R. Peterman
Lonnie G. Olson
Gary S. Groenewold
Rocklan G. McDowell
Richard D. Tillotson
Jack D. Law

August 2013

The INL is a U.S. Department of Energy National Laboratory
operated by Battelle Energy Alliance

INL/EXT-13-29727
FCRD-SWF-2013-000202

Characterization of Radiolytically Generated Degradation Products in the Strip Section of a TRUEX Flowsheet

Dean R. Peterman
Lonnie G. Olson
Gary S. Groenewold
Rocklan G. McDowell
Richard D. Tillotson
Jack D. Law

August 2013

Idaho National Laboratory
Fuel Cycle Research & Development
Idaho Falls, Idaho 83415

http://www.inl.gov

Prepared for the
U.S. Department of Energy
Office of Nuclear Energy
Under DOE Idaho Operations Office
Contract DE-AC07-05ID14517

SUMMARY

This report presents a summary of the work performed to meet the FCRD level 2 milestone M3FT-13IN0302053, "Identification of TRUEX Strip Degradation." The effects of gamma radiolysis upon the efficacy of the strip section of a TRUEX flowsheet for the recovery of trivalent actinides and lanthanides from acidic solution were determined by a combination of static and test loop irradiations. Compositions of the irradiated aqueous and organic solutions were determined using a suite of analytical techniques. In addition, ESI-MS was used to identify some of the products of the radiolytic degradation of lactic acid, DTPA, CMPO, and TBP.

For lactic acid, the major degradation products detected by ESI-MS were pyruvic acid and a species corresponding to a lactic acid-pyruvic acid cluster. The major product of DTPA degradation was determined by ESI-MS to be a DTPA lactam resulting from the radiolytic loss of glycolic acid. Acetate and several other unknown degradation products of both lactic acid and DTPA were detected by HPLC analysis. Several species arising from the degradation of CMPO ($[(iBu)_2NPrH]^+$, $[(iBu)_2PrH_2]^+$ and CMPO-carboxylic acids) were determined by ESI-MS; which is consistent products identified in previous studies.

The generally lower *G*-values determined for test loop irradiation compared to static irradiation experiments clearly points out the importance of performing radiolytic degradation studies using oxygenated, mixed aqueous and organic solutions. The actual mechanism by which dissolved oxygen present in the test loop ameliorates the radiolytic degradation is not known. However, the rapid reaction of oxygen with carbon centered radicals would produce less reactive peroxyl radicals. Further studies are necessary in order to develop a complete understanding of the role played by dissolved oxygen in the inhibition of radiolytic degradation of solvent extraction process solvents.

Gamma radiolysis results in a small increase the distribution ratios in the strip section of the TRUEX flowsheet (D_{Am} = <0.001 at 0 kGy absorbed dose to D_{Am} = 0.015 at 1300 kGy absorbed). Even the distribution ratio determined for the highest absorbed dose is not expected to adversely impact operation of the stripping section of the TRUEX flowsheet. However, the generation of degradation products in the aqueous phase and the radiolytic destruction of lactic acid and DTPA may have serious impacts on a subsequent TALSPEAK process. Close coupling of the TRUEX and TALSPEAK operations may help to mitigate these effects by limiting the gamma dose to the strip product solution.

CONTENTS

FIGURES

TABLES

ACRONYMS

AMUSE	Argonne Model for Universal Solvent Extraction
CID	Collision-induced dissociation
CINC	Costner Industries Nevada Corporation
CMPO	Octyl(phenyl)-N, N-diisobutylcarbamoylmethyl phosphine oxide
HDBP	Dibutylphosphoric acid
DTPA	Diethylenetriaminepentaacetic acid
EDTA	Ethylenediaminetetraacetic acid
ESI-MS	Electrospray ionization mass spectrometry
FCR&D	Fuel Cycle Research and Development program
IC	Ion chromatography with conductivity detection
INL	Idaho National Laboratory
LA	Lactic Acid
LET	Linear energy transfer
H_2MBP	Monobutylphosphoric acid
O/A	Organic to aqueous phase ratio
PUREX	Plutonium Uranium Reduction Extraction
TALSPEAK	Trivalent Actinide Lanthanide Separation by Phosphorous reagent Extraction from Aqueous Komplexes
TBP	Tri-butylphosphate
TRUEX	Trans Uranic Extraction

SEPARATIONS CAMPAIGN

CHARACTERIZATION OF RADIOLYTICALLY GENERATED DEGRADATION PRODUCTS IN THE STRIP SECTION OF A TRUEX FLOWSHEET

1. Introduction

The radiolysis/hydrolysis test loop, located at the Idaho National Laboratory (INL), was utilized to study the impacts of radiolytic and hydrolytic degradation products on the performance of the stripping section of the TRansUranic EXtraction (TRUEX) process. The TBP/alkane diluent system has received extensive attention in the scientific literature for at least the last forty years. The radiation chemistry of the TBP was recently reviewed by Mincher and co-authors.[1, 2] Further, Mincher *et al.* have also recently reviewed the radiation chemistry of organophosphorus extractants such as octylphenyl-N,N-diisobutylcarbamoylmethyl phosphine oxide (CMPO), one of the components of the TRUEX process solvent.[3]

The current TRUEX flowsheet concept considered by the Fuel Cycle Research Development program is intended to separate the trivalent actinides and lanthanides from the Raffinate of a U/Pu separation process. The trivalent actinides would then be separated from the lanthanides using the Trivalent Actinide Lanthanide Separation by Phosphorous reagent Extraction from Aqueous Komplexes (TALSPEAK). The TALSPEAK process requires an aqueous phase containing a polyaminopolycarboxylate actinide holdback reagent and an organic acid buffer. The TALSPEAK flowsheet employs 1.5 M diethylenetriaminepentaacetic acid (DTPA) as the holdback reagent and 0.050 M lactic acid (LA) as the buffer in the aqueous phase of the extraction section. Therefore, the TRUEX flowsheet evaluated in this report used a mixture of 1.5 M DTPA and 0.050 M LA as the aqueous stripping reagent.

The successful deployment of any solvent extraction ligand proposed for use in fuel cycle separations will depend upon the stability of that ligand in an acidic, radioactive environment. Irradiation of the ligand occurs due to the decay energy of actinides and fission products in the dissolved nuclear fuel solution. The radiation types are predominantly low linear energy transfer (LET) beta/gamma radiation from fission product decay, and high LET alpha radiation from actinide decay. The major reactive species formed [4] by radiolysis of water, alkane diluent, and nitric acid are shown in Equations 1 – 3, respectively.

$$H_2O \text{ -}\backslash\!/\backslash\!/\backslash\!\rightarrow {}^{\bullet}OH + e^{-} + H^{\bullet} + H_2O_2 + H_3O^{+} + H_2 \quad (1)$$

$$CH_3(CH_2)_nCH_3 \text{ -}\backslash\!/\backslash\!/\backslash\!\rightarrow e^{-}_{sol} + CH_3(CH_2)_nCH_3^{\bullet+} + CH_3(CH_2)_nCH_2^{\bullet} + {}^{\bullet}CH_3 + H^{\bullet} + H_2 \quad (2)$$

$$HNO_3 \text{ -}\backslash\!/\backslash\!/\backslash\!\rightarrow {}^{\bullet}NO_2 + {}^{\bullet}NO_3 + , HNO_2 \quad (3)$$

Equations 1 – 3 show that radiolysis of aqueous and organic phases generates a range of oxidizing ($^{\bullet}OH$, $^{\bullet}NO_3$, $^{\bullet}NO_2$) radicals, reducing ($H^{\bullet}$) radicals, the reducing aqueous electron (e^{-}_{aq}), and reactive molecular species (H_2O_2, HNO_2, H_2).

Due to the relatively low ligand concentrations employed most decay energy is absorbed by the diluent, and ligand radiolysis is expected to occur by indirect, rather than direct mechanisms. For example, the proposed TRUEX solvent contains 0.2 M CMPO as the ligand, while the tributylphosphate (TBP) modifier and dodecane diluent concentrations are about 1.4 M and 3 M, respectively. Consequently, most ligand damage will be due to reaction with reactive species created by energy deposition in the balance of the organic phase, or in the acidic aqueous phase in contact with that organic phase. Therefore, realistic examination of the impacts of radiolytic degradation upon the efficacy of solvent extraction processes used in an advanced nuclear fuel cycle, necessitates studying the radiolysis of mixed aqueous and organic systems.

2. Experimental Methods

2.1 Radiolysis and Hydrolysis Test Loop

The irradiation source (see Figure 1) is a MDS Nordion GammaCell 220 Excel self-contained ^{60}Co gamma irradiator. The center-line gamma dose rate in the sample chamber is ~5.7 kGy/hr. The solvent irradiation loop is based upon a coil of borosilicate glass tubing (0.375" OD, 0.202" ID) which is placed in the gamma irradiator sample chamber. The effective absorbed gamma dose rate of 3.3 kGy/hr delivered to samples in the test loop was based upon decay-corrected Fricke dosimetry, [5] the photo-bleaching of a methyl red solution due to gamma irradiation,[6] and the duration of each irradiation. During the solvent irradiation, the aqueous and organic phases are mixed using a centrifugal contactor (CINC V-02, USA) with the rotor replaced by a four vane mixing paddle. The interior of the centrifugal contactor housing may be purged with inert gas, if necessary. The organic and aqueous phases used are metered into the mixing region of the contactor at the desired organic to aqueous phase ratio (O/A). The mixed phases are pumped through the irradiator test loop by a magnetic drive gear pump. The mixed phases flow through the glass coil in the irradiator sample chamber, through an external coil in a water bath, and return to the inlet of the centrifugal contactor where the phases are mixed and circulated back through the loop. In-line tube mixers (TAH Industries, Inc.) are used to provide additional phase mixing in the test loop. The in-line tube mixers are placed between the outlet of the gear drive pump and the inlet of the irradiation loop and between the outlet of the irradiation loop and the inlet to the external temperature control coil. The flowrate of the dispersion is in the range of 1.5 L/min in order to maintain turbulent flow and keep the phases dispersed. The radiolysis/hydrolysis test loop is equipped with pressure gauges and thermocouples before and after the gamma irradiator. Two flow sight glasses are used to monitor the extent of mixing in the test loop. The two phases continue to circulate until the desired dose is obtained.

Figure 1. MDS Nordion GammaCell 220 gamma irradiator.

The temperature inside the sample chamber is ~38 °C due to the decay heat of the ^{60}Co source. A temperature-controlled water bath (external to the sample chamber) is used to maintain the desired temperature of the test solutions within the test loop. The sampling port permits samples to be withdrawn from the test loop in order to monitor the conditions during an irradiation. To facilitate hydrolysis of the solvent in the test loop, this setup will allow the solution to be maintained at an elevated temperature throughout testing if desired. A flow cell and dissolved oxygen sensor was added in FY-2012 in order to

monitor the amount of oxygen present in the test loop solution during gamma radiolysis or without gamma radiolysis. A schematic view of the test loop is shown in Figure 2.

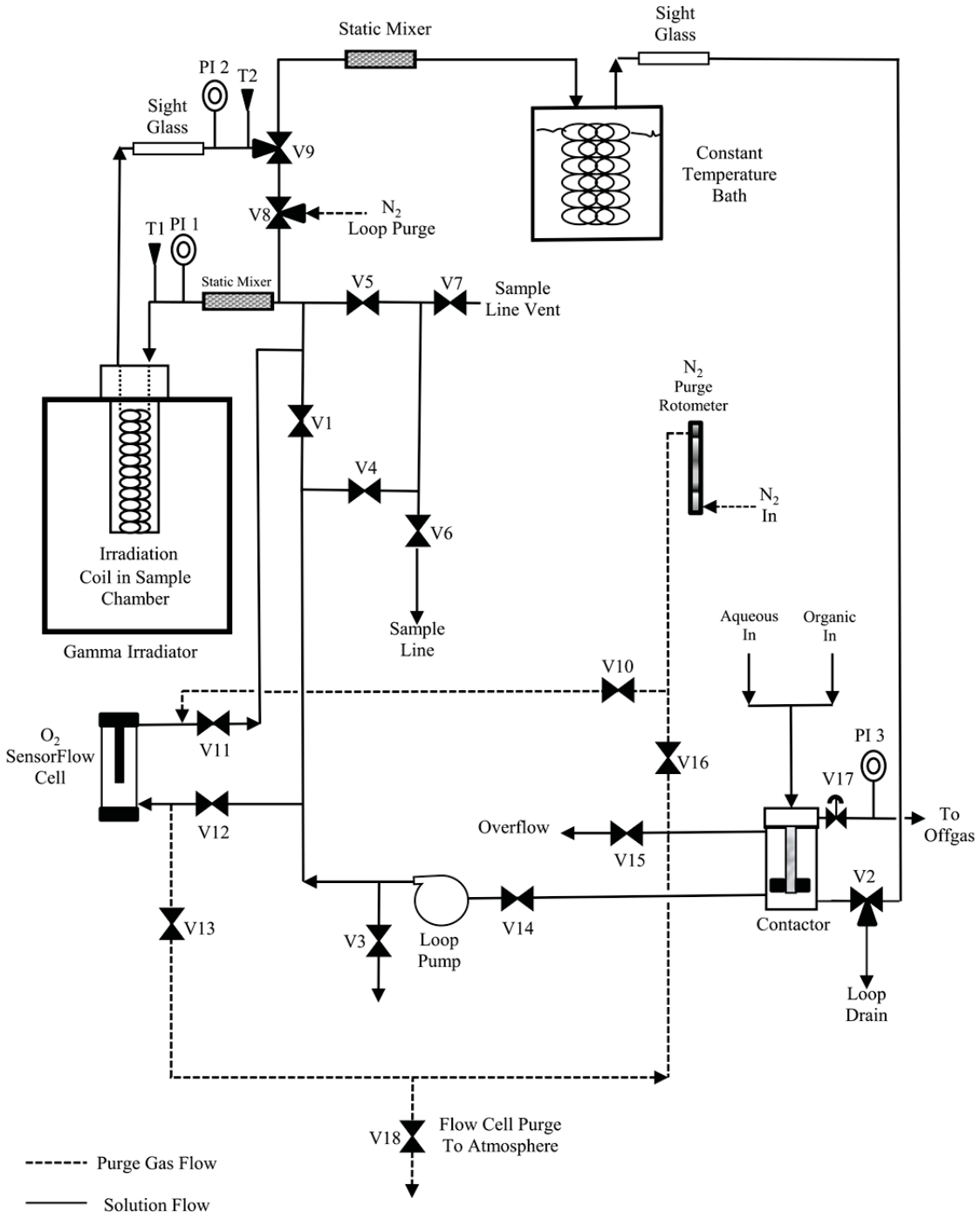

Figure 2. Schematic diagram of the INL Radiolysis and Hydrolysis Test Loop.

Samples were also irradiated in a static configuration. For static irradiation experiments, samples (aqueous, organic, or aqueous and organic) are sealed in capped scintillation vials and exposed to gamma irradiation using the GammaCell 220E irradiator which is equipped with a jig to hold the vials in fixed

positions. The gamma dose rate delivered to each position on the irradiation jig was determined by standard Fricke dosimetry.[5]

The efficiency of the conversion of absorbed radiation energy (gamma rays) into chemical products is defined here as the *G*-value, in units of $\mu mol \cdot L^{-1} \cdot Gy^{-1}$. A *G*-value can be used to predict the extent of radiolytic degradation of a solvent component for a given absorbed dose. The irradiated organic samples were analyzed by GC-FID and HPLC in order to determine the composition of the solvent as a function of absorbed dose. The GC-FID and HPLC analyses also permitted the identification and quantification (in some cases) of organic soluble radiolytic degradation products. The irradiated aqueous samples were analyzed by IC and HPLC in order to determine the composition of the aqueous TRUEX stripping reagent as a function of absorbed dose. Aqueous phase soluble radiolytic degradation products were identified and in some cases quantified as a function of absorbed dose.

2.2 Gas Chromatographic Analysis

Samples of TRUEX solvent were analyzed by gas chromatography with flame ionization detection (GC-FID) for the presence of potential degradation products as well as tri-*n*-butylphosphate (TBP).

Due to the acidic functional groups of the dibutylphosphoric acid (HDBP) and monobutylphosphoric acid (H_2MBP) degradation products of TBP, an aliquot of each TRUEX solvent sample was diluted 100 fold with hexane and derivatized with 300 µL of an ~0.3 mol/L solution of diazomethane in hexane prior to analysis.[7] This produced the methyl ester of the phosphoric acid functional groups in the target compounds. Due to the large concentration of TBP relative to HDBP or H_2MBP present, samples for TBP analysis were diluted 10,000 fold with hexane. The samples were analyzed along with appropriate calibration and quality assurance samples for TBP and the derivatized potential degradation products via GC-FID.

The gas chromatography analyses were performed on a Thermo Scientific Trace ULTRA gas chromatograph. The chromatograms were processed using Thermo Scientific Xcalibur software. The chromatographic separations were carried out utilizing a Thermo Scientific TG-35MS capillary column (30m x 0.32mm ID x 0.5µm film). Analytical conditions were set at 2.0 mL/min constant flow with helium as the carrier gas and an 80 mL/min split flow. Oven operating conditions started with a 2 min hold at 70°C, followed by a ramp at 20°C/min to 240°C then 40°C/min to 280°C, finished with an 8.25 min hold at 280°C. A Thermo AS3000 auto sampler was used for all injections, employing a 1 µL hot injection with the inlet set at 250 °C and 5 second pre-injection dwell time. The FID was held constant at 250°C. The fuel gas for the FID is a mixture of 350 mL/min air and 35 mL/min hydrogen with 30 mL/min nitrogen as a makeup gas.

2.3 Ion Chromatographic Analysis

A Dionex (Sunnyvale, CA, USA) ICS-5000 ion chromatograph equipped with an eluent generator, an autosampler, a quaternary gradient pump with degasser, conductivity detector, an anion self-regenerating suppressor (ASRS), a CR-ATC continuously regenerated anion trap column, and an ASRS 300 anion suppressor was used for all IC experiments. All columns and other consumables were obtained from Dionex. Either an IonPac AS5A analytical column (4mm x 150mm) with IonPac AG5A guard column (4mm x 35mm) or IonPac AS-11HC (2mm x 250mm) with AG-11HC guard column (2mm x 50mm) were used. The flow rate was isocratic at 1.0 mL/min (4mm column) or 0.38 mL/min (2mm column). The step gradient was maintained using an EluGen II KOH cartridge and eluent generator. IC quality water (Fluka) was used for the preparation of all eluents, standards, and samples.

The procedure used for the IC analysis of the aqueous samples is based upon the work of Dodi and Verda.[8] Due to the varying concentration of the analytes present in the irradiated samples, an aliquot of each aqueous sample was diluted between 5 and 200 fold with water. The samples were analyzed along with appropriate calibration and quality assurance samples. The KOH eluent concentration determined for elution of expected constituents of aqueous phase samples is given in Table 1.

Table 1. KOH eluent concentration corresponding to elution of analyte ions in IC analysis.

Analyte of Interest	$[OH^-]$, mM
Lactate ion and HDBP ion	3.0-5.0
H_2MBP ion	15.0-23.0
Phosphate ion	50.0-55.0

2.4 High Performance Liquid Chromatographic Analysis

High Performance Liquid Chromatography (HPLC) was used to quantify CMPO in the irradiated TRUEX solvent. The HPLC analyses for determination of CMPO concentration were performed using a Dionex (Sunnyvale, CA, USA) ICS-5000 ion chromatograph equipped with an autosampler, a quaternary gradient pump with degasser, a photo-diode array detector, and Chromeleon 7 software. All HPLC experiments were carried out isocratically using a mixture of 30 mM phosphate buffer (pH ~2.6) and 2-propanol containing 3.6 % 1-octanol in a 60/40 ratio. The chromatographic separation was achieved with a C_{18} reverse-phase (RP-C_{18}) column (Supelco, 25 cm x 4.6 mm, 5 μm) with a flow rate of 1 mL /min. The column temperature was maintained at 50º C. The CMPO concentration was determined at a wavelength of 220 nm.

Samples of irradiated TRUEX solvent were diluted between 25 and 200 fold due to variations in CMPO and degradation product concentration. The samples were analyzed along with appropriate calibration and quality assurance samples.

The concentration of DTPA present in the irradiated samples was determined by HPLC analysis. The HPLC system used for these analyses consisted of a Waters Model 717 Autosampler with a Model 600e Multisolvent Delivery Pump System and Model 2996 photodiode array detector. The separation was performed using a SIELC 4.6x250 mm PrimeSep D column with 5 μm particles and 100 Å pores using a gradient consisting of 100% solvent A to 100% solvent B over 12 min, ramp back to 100% A over 1 minute and holding for 7 minutes. An additional 6 minutes for re-equilibration was allowed between sample injections. Solvent A was 10% acetonitrile/90% water with the addition of 2 μL/L concentrated sulfuric acid and 0.02% (w/w) $CuSO_4$. Solvent B was 50% acetonitrile/50% water with the addition of 20 μL/L concentrated sulfuric acid and 0.02% (w/w) $CuSO_4$.

2.5 Electrospray Ionization-Mass Spectrometry (ESI-MS)

Prior to ESI analysis the 10 microLiter samples were diluted by 1000 with MeOH. The diluted solutions were analyzed using ESI-MS in positive ion mode using a micrOTOF-QII mass spectrometer (Bruker, Billerica, MA, USA). Samples were introduced by direct infusion using a gas-tight syringe driven by a syringe pump at a rate of 3 μL min^{-1} connected to the ESI capillary by polyether ether ketone tubing. The temperature of the ESI source capillary was maintained at 180 °C, with the source potential at 4.5 kV. Electrosprayed ions are transferred from the ESI-MS source to a high-resolution time-of-flight

mass analyzer by an ion optical train consisting of an ion funnel, a hexapole, a quadrupole and finally a quadrupole collision cell. Collision induced dissociation (CID) is accomplished by performing mass selection using the first quadrupole, ion dissociation in the collision cell, and finally fragment ion measurement using the time-of-flight analyzer. The collision energy was empirically controlled by varying the potential on the collision cell.

3. Results and Discussion

The INL test loop has previously been used to evaluate the effects of hydrolytic and radiolytic degradation upon the efficacy of the extraction[9] and stripping[10] sections of the TRUEX flowsheet. The nominal composition of the TRUEX solvent used in these studies is 0.2 M CMPO and 1.4 M TBP dissolved in n-dodecane. The TRUEX stripping solution is comprised of a mixture of lactic acid and diethylenetriaminepentaacetic acid (DTPA). The static irradiations were used to explore the importance of different suites of radical species formed in the absence and presence of an organic phase. The test loop irradiations were performed to most closely approximate conditions expected in an actual process. Due to production of hydrated electrons, small absorbed doses (< 1 kGy) resulted in the consumption of any oxygen dissolved in the static irradiation samples. Since the test loop was exposed to an ambient atmosphere, the effect of dissolved oxygen upon the observed distribution of degradation products was examined by comparison of the static and test loop irradiations.

Experiments performed during FY-2012 demonstrated that gamma radiolysis does cause a small decrease of the americium and europium distribution ratios in the extraction section as absorbed dose increases, but this decrease would likely not adversely impact performance. The INL test loop was also used to evaluate the strip section of the TRUEX flowsheet. The impact of gamma irradiation was evaluated by the determination of the variation of the americium distribution ratio as a function of absorbed dose. [10] The observed increase in americium stripping distribution ratios suggests the radiolytic production of organic soluble degradation compounds that will complex metal ions, i.e. americium. While the observed increases are statistically significant, the increase from D_{Am} = <0.001 at 0 kGy absorbed dose to D_{Am} = 0.015 at 1300 kGy absorbed dose is not expected to adversely impact process operation.

Samples from the static irradiations of TRUEX aqueous strip only and TRUEX aqueous strip plus TRUEX solvent and TRUEX strip section test loop irradiation were generated during FY-2012. These samples were analyzed in order to determine sample composition and to identify radiolytic degradation products during FY-2013.

3.1 Description of Typical Analytical Results

Samples of irradiated TRUEX solvent were analyzed by GC-FID in order to determine the variation in the composition of the solvent due to radiolytic degradation. A typical GC-FID chromatogram observed for the analysis of TBP is shown in Figure 3. In the chromatogram, n-dodecane and TBP elute at RT = 6.5 min and 10.4 min, respectively. The peak at RT = 8.5 min corresponds to 2-dodecanol which is used as an internal injection standard. However, the radiolytic production of dodecanol at high absorbed dose (presumably due to diluent radiolysis) limited the effectiveness of 2-dodecanol as an injection standard. A typical chromatogram observed for the analysis of HDBP and H_2MBP is shown in Figure 4. Under the conditions employed for the analysis of acidic degradation products, the observed RT for n-dodecane and TBP are shifted to higher values due to the large amount of these species injected onto the GC column.

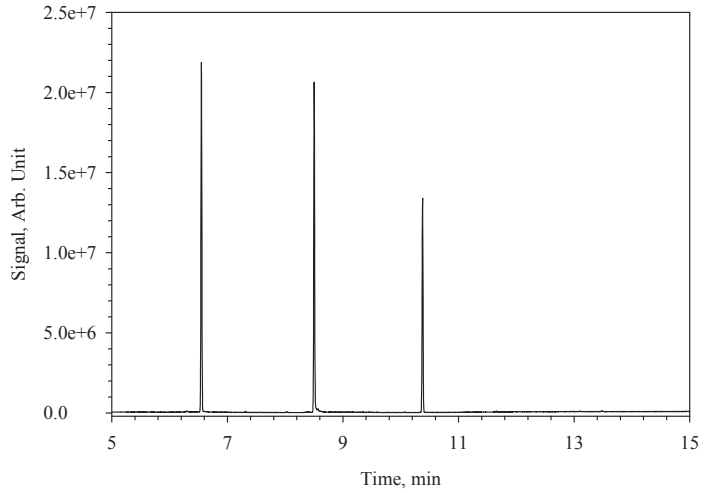

Figure 3. Typical GC-FID chromatogram for TBP analysis. Retention times: RT = 6.5 min, n-dodecane; RT = 8.5 min, 2-dodecanol; RT = 10.4 min, TBP.

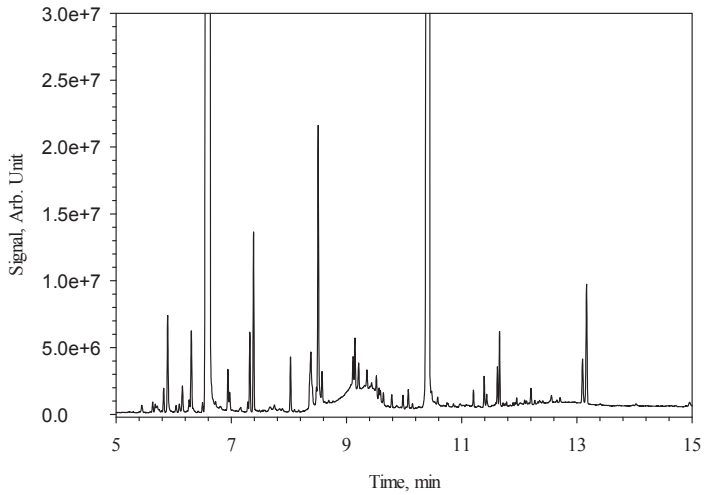

Figure 4. Typical GC-FID chromatogram for HDBP and H_2MBP analysis. Retention times: RT = 7.6 min, methyl ester of H_2MBP; RT = 9.2 min, methyl ester of HDBP.

In addition to the GC techniques used to determine the composition of organic solvents, samples of irradiated aqueous phase were analyzed by anion chromatography to determine aqueous soluble degradation products. Figure 5 shows a typical ion chromatograph showing the response for lactate, RT = 4 min; HDBP, RT = 10.5 min; H_2MBP, RT = 15 min; and phosphate, RT = 18.5 min. Due to wide range of concentrations of degradation products formed, several analyses were required to quantify all of these anions.

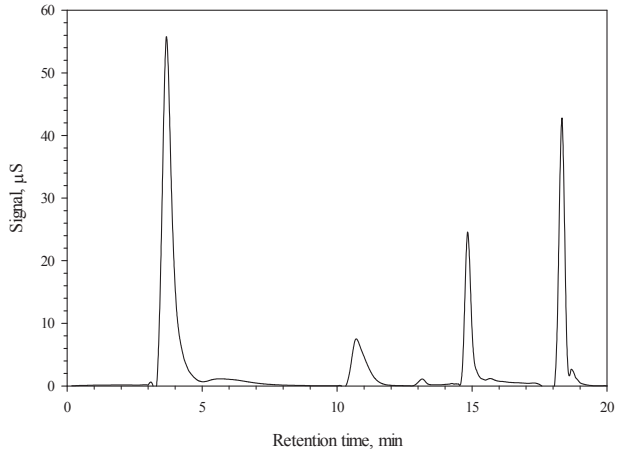

Figure 5. Ion chromatograph – RT = 4 min, lactate; RT = 10.5 min, HDBP; RT = 15 min, H_2MBP; RT = 18.5 min, phosphate.

A typical IC chromatogram corresponding to the analysis of an aqueous sample of irradiated TRUEX stripping reagent is shown in Figure 6. The peak due to lactate anion is off scale due to the high lactic acid concentration in these samples. Peaks attributable to HDBP and H_2MBP are clearly resolved. The peaks at RT ~ 7 min and RT ~ 12.5 min correspond to unidentified degradation products. The group of peaks around RT ~ 18 min corresponds to phosphate and at least two other unidentified degradation products which appear to co-elute with phosphate. The presence of these co-eluting peaks complicated the analysis of phosphate formed in the irradiated TRUEX stripping solutions.

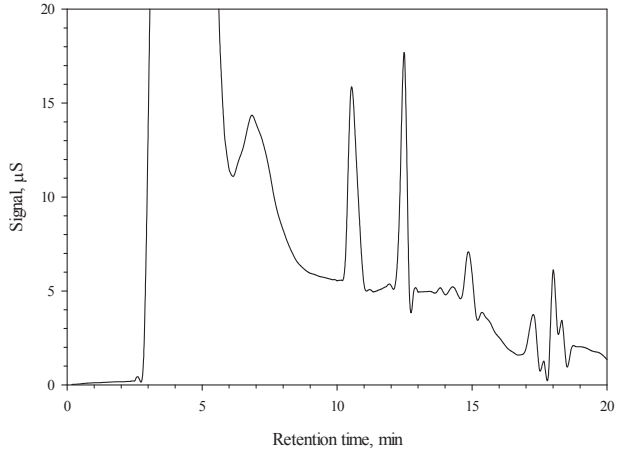

Figure 6. Ion chromatograph – RT = 4 min, lactate; RT = 6.5 min, unknown; RT = 10.5 min, HDBP; RT = 12.5 min, unknown; RT = 15 min, H_2MBP; RT = 17 – 19 min, unknowns and phosphate.

The organic phases from the TRUEX radiolysis experiments were analyzed by HPLC in order to determine the concentration of CMPO and presence of other organic soluble radiolytic degradation products. A typical set of HPLC chromatograms are shown in Figure 7. The peak corresponding to CMPO has a retention time of 19.0 min. The peaks at retention times of 6.1 min, 9.8 min, 10.3 min and 15.9 min, respectively, are unidentified radiolytic degradation products.

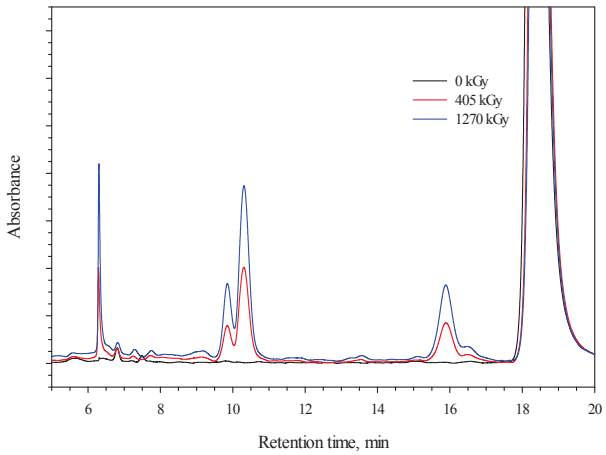

Figure 7. Typical HPLC chromatograms for the analysis of CMPO in TRUEX solvent irradiated in contact with TRUEX stripping reagent in the test loop. Retention times: unknown 1, RT = 6.1 min; unknown 2, RT = 9.8 min; unknown 3. RT = 10.3 min; unknown 4, RT = 15.9 min; CMPO, RT = 19.0 min.

The aqueous phases from the TRUEX radiolysis experiment were also analyzed by HPLC in order to determine the concentration of DTPA and presence of other aqueous soluble degradation products. A typical set of HPLC chromatograms is shown in Figure 8. The lactate component present in the TRUEX stripping reagent elutes at 4.8 min and the DTPA component elutes at 7.5 min.

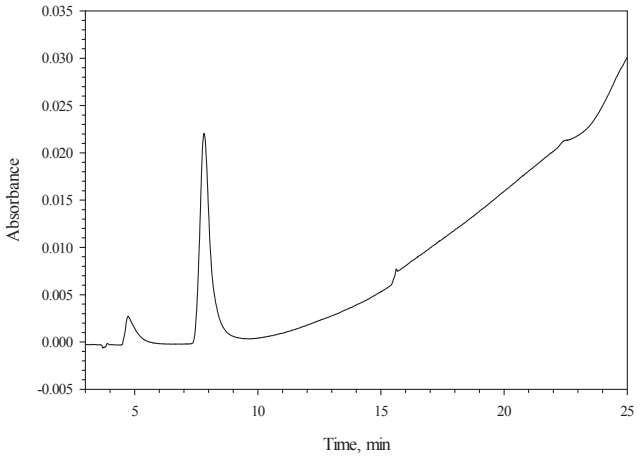

Figure 8. Typical HPLC chromatogram of aqueous TRUEX stripping reagent. Retention times: 4.7 min, lactate; 7.9 min, DTPA.

The HPLC chromatograms from the test loop irradiation of the TRUEX strip section are shown in Figure 9. These chromatograms clearly show the decrease in the concentration of DTPA with increasing dose. Due to the lower sensitivity compared to the IC method, lactic acid was not quantified using this HPLC method. At least four degradation products appear in the chromatograms with increasing dose. The peak at a retention time, RT = 4.3, was assigned to acetate anion using known standards. The peaks at retention times, RT = 3.4, 6.2, and 6.7 min, could not be identified using known standards.

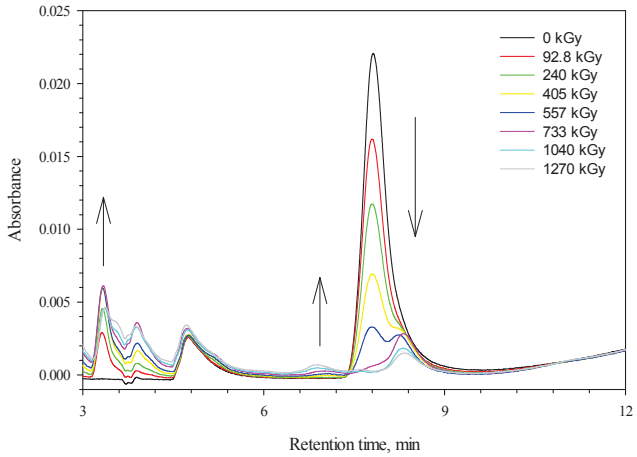

Figure 9. HPLC analysis of the aqueous phase from the test loop irradiation of TRUEX strip solution in contact with TRUEX solvent. Retention times: 4.7 min, lactate; 7.9 min, DTPA.

3.2 Static Irradiation of Aqueous TRUEX Strip Solution

The nominal composition of the TRUEX stripping solution is 1.5 M LA and 0.050 M DTPA. In the TRUEX flowsheet, the pH of this solution is adjusted to pH = 3.5. Initially the aqueous stripping solution alone was irradiated in sealed vials. The irradiated solutions were then analyzed to determine the change in component concentration with absorbed dose. The decrease in LA and DTPA concentration as a function of absorbed dose for the static irradiation of the TRUEX stripping solution are presented in Figures 10 and 11, respectively.

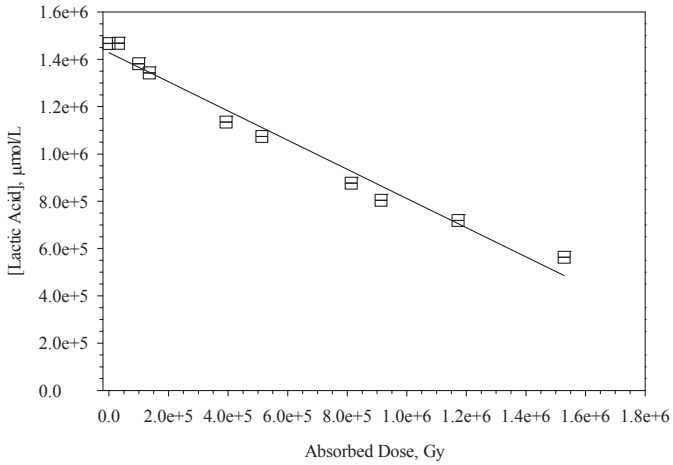

Figure 10. Concentration of lactic acid determined by IC analysis as a function of absorbed dose for the static irradiation of aqueous TRUEX stripping reagent. The slope of the linear best-fit line corresponds to a *G*-value for the radiolytic degradation of LA of $-G_{LA} = -0.617 \pm 0.033$ µmol·L^{-1}·Gy^{-1}. ($R^2 = 0.98$).

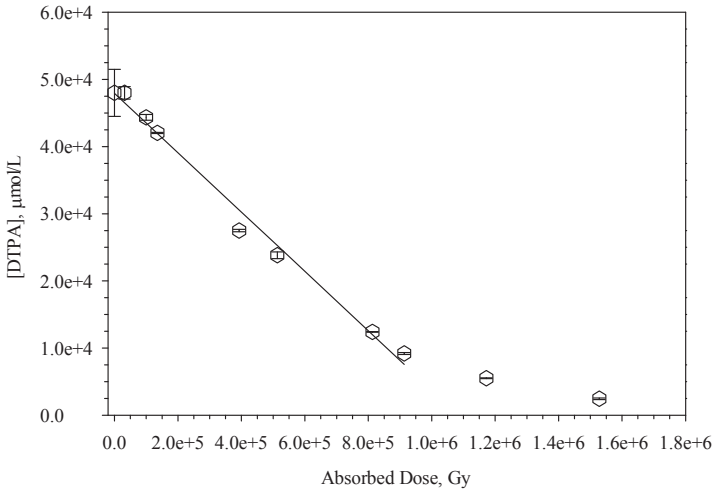

Figure 11. Concentration of DTPA determined by HPLC analysis as a function of absorbed dose for the static irradiation of aqueous TRUEX stripping reagent. The slope of the linear best-fit line corresponds to a *G*-value for the radiolytic degradation of $-G_{DTPA}$ = -0.044 ± 0.002 µmol·L^{-1}·Gy^{-1}. (R^2 = 0.99).

The static irradiation of the TRUEX stripping solution in the absence of TRUEX solvent causes significant radiolytic degradation of lactic acid and DTPA. At the highest absorbed dose studied, the concentration of lactic acid has decreased by approximately 50 % and the DTPA concentration has decreased to nearly undetectable levels. The *G*-value for the radiolytic degradation of LA, $-G_{LA}$ = -0.617 ± 0.033 µmol·L^{-1}·Gy^{-1}. This *G*-value is quite large and cannot be explained only by the reaction of lactic acid with a radiolytically produced radical species. However, Bibler [11] studied the gamma irradiation of DTPA dissolved in 4 M HNO_3 and reported $-G_{DTPA}$ = ~0.5 µmol·L^{-1}·Gy^{-1} (assuming ρ = 1 g/mL). The large *G*-value may be attributable to a chain reaction in which a product of the reaction of LA and a radical species undergoes further reaction with lactic acid in the aqueous phase. Based upon scavenger experiment, the majority of DTPA degradation was attributed to hydroxyl ($^{\bullet}$OH) radical (k = 2 x 10^9 mol·L^{-1}·s^{-1} at pH = 6).

The *G*-values determined for the static irradiation of the aqueous TRUEX strip reagent are summarized in Table 2.

Table 2. *G*-values determined for the static irradiation of the aqueous TRUEX strip reagent.

Species	*G*-value, µmol·L^{-1}·Gy^{-1}	R^2
Lactic Acid	-0.617 ± 0.033	0.98
DTPA	-4.42 x 10^{-2} ± 1.49 x 10^{-3}	0.99

Electrospray ionization mass spectrometry (ESI-MS) was used to attempt to explain the effects of gamma radiolysis upon the static irradiated aqueous strip solution. Only a summary of the ESI-MS results are presented. A detailed description of the ESI-MS results is available in the Appendix.

The positive ion spectrum of the zero absorbed dose sample contained low abundance ions corresponding to intact LA in the form of $[(LA)Na]^+$ and $[(LA\text{-}H)Na_2]^+$ at *m/z* 113 and 135. In addition, more abundant ions at *m/z* 185 and 257 were observed which correspond to esters of LA which are also present in the lactic acid stock solution and thus are not a product of radiolysis. The DTPA furnished a

protonated molecular ion $[(DTPA)H]^+$ at *m/z* 394 and natiated (sodium containing) ions at *m/z* 416 and 438.

As the absorbed dose increases two new ions are observed at *m/z* 318 and 340 that are unequivocally derived from DTPA degradation. The DTPA degradation product has a lactam structure (see Figure 12). This structure supported by accurate *m/z* measurements, which are consistent with the proposed elemental composition and by collision induced dissociation (CID) reactions (see Appendix).

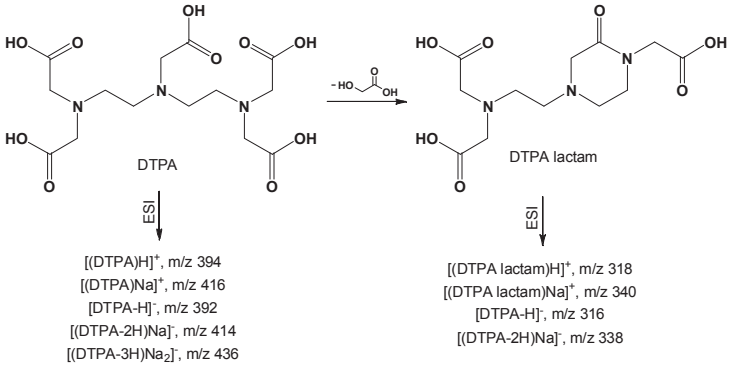

Figure 12. Radiolytic degradation of DTPA to form the DTPA lactam.

Höbel and von Sonntag[12] used pulsed radiolysis to generate $^{\bullet}OH$ radical and study the degradation of EDTA by the hydroxyl radical in aqueous solution. They reported the formation of both N- and carbon-centered radical species. The N-centered radicals decayed to form reducing carbon-centered radicals by deprotonation or electron transfer from a carboxylate group. While these authors did not propose a lactam structure to explain the EDTA degradation, the generation of N- and C-centered radicals would account for the DTPA lactam degradation product observed in this study. A similar mechanism was proposed by Bibler[11] in which decarboxylation occurs via formation of a six-membered promoted by a an exchange reaction between a carboxylate group and $^{\bullet}OH$ radical.

With increasing dose, both the LA and the lactic acid esters decompose with subsequent formation of ions derived from LA-pyruvic acid and lactic acid ester-pyruvic acid compounds. Plots of ion intensities as a function of absorbed dose for LA, DTPA, and DTPA lactam derived ions are presented in Figures 13 – 15, respectively. For the degradation of LA and DTPA, the plotted ion intensities correspond with the analytical results. The plot of ion intensity versus absorbed dose for the DTPA lactam product indicates that the lactam undergoes further radiolytic degradation. The lactam degradation products have not been identified.

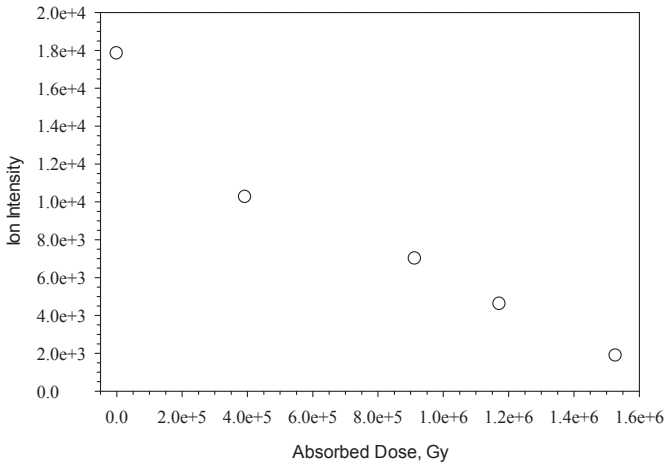

Figure 13. Positive ion intensity versus absorbed dose corresponding to ions derived from LA and lactic acid esters for the static irradiation of the TRUEX aqueous strip solution.

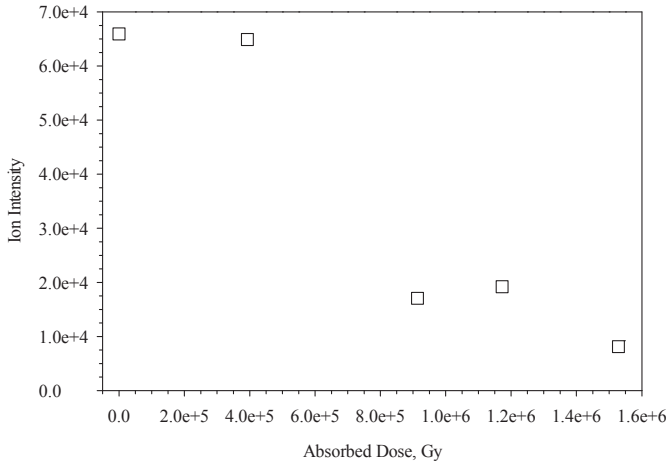

Figure 14. Positive ion intensity versus absorbed dose corresponding to ions derived from DTPA for the static irradiation of the TRUEX aqueous strip solution.

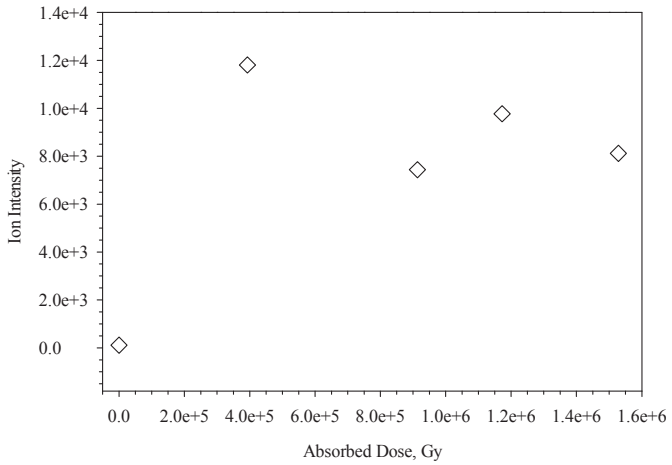

Figure 15. Positive ion intensity versus absorbed dose corresponding to ions derived from DTPA lactam for the static irradiation of the TRUEX aqueous strip solution.

The negative ion ESI of the static irradiated TRUEX aqueous strip phase revealed similar results for LA and DTPA. Interestingly, two new LA degradation products were identified. These products correspond to pyruvic acid and a LA-pyruvate adduct. Pyruvic acid is the dicarboxylic acid analogue of LA. Plots of negative ion intensities as a function of absorbed dose for the pyruvic acid and LA-pyruvate adduct are presented in Figures 16 and 17, respectively. The ions corresponding to pyruvic acid and the LA-pyruvate adducts are detected at zero absorbed dose; suggesting that these species are generated to some extent by the ESI technique. However, the steady increase in the intensity of both ions with increasing dose suggests that a radiolytic production process is reasonable. Further studies are necessary to determine if the formation of the LA-pyruvate cluster may explain the unusually high *G*-value for the radiolytic degradation of LA determined for the static irradiation of the TRUEX aqueous strip solution.

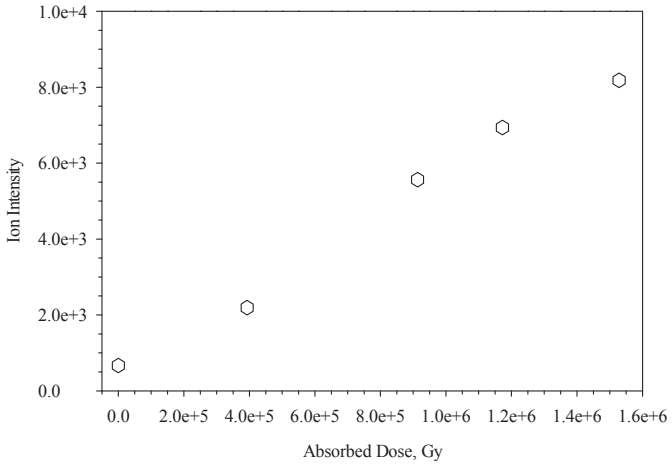

Figure 16. Negative ion intensity versus absorbed dose corresponding to pyruvic acid ions derived from lactic acid degradation for the static irradiation of the TRUEX aqueous strip solution.

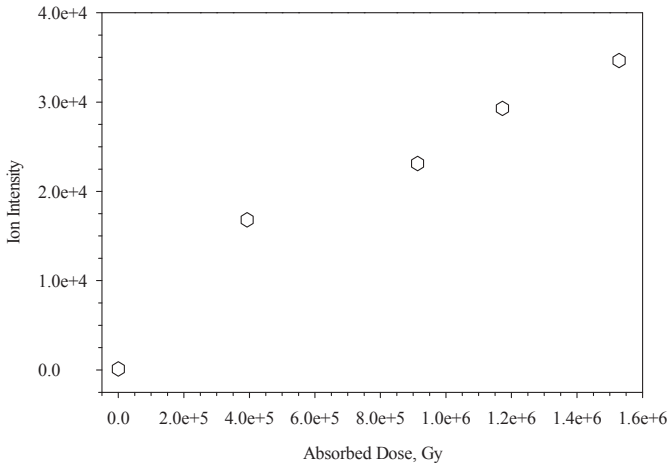

Figure 17. Negative ion intensity versus absorbed dose corresponding to LA-pyruvate adduct ions derived from lactic acid degradation for the static irradiation of the TRUEX aqueous strip solution.

3.3 Static Irradiation of TRUEX Strip Solution and TRUEX Solvent

Static irradiations of the TRUEX stripping solution in contact with TRUEX solvent were performed and both the aqueous and organic phases were analyzed. Radiolytic degradation products were identified and quantified where possible. The variation in the concentration of LA and DTPA present in the aqueous phase of the mixed phase static irradiation of the TRUEX strip section are shown in Figures 18 and 19, respectively.

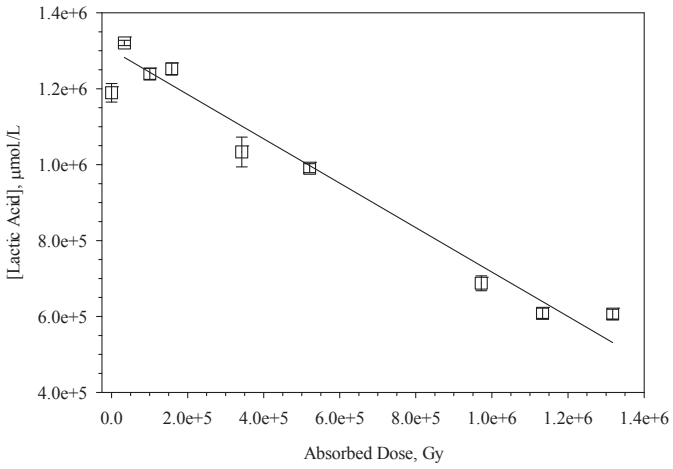

Figure 18. Concentration of lactic acid determined by IC analysis as a function of absorbed dose for the static irradiation of aqueous TRUEX stripping reagent in contact with TRUEX solvent. The slope of the linear best-fit line corresponds to a *G*-value for the radiolytic degradation of $-G_{LA} = -0.583 \pm 0.040$ µmol·L^{-1}·Gy^{-1}. ($R^2 = 0.97$).

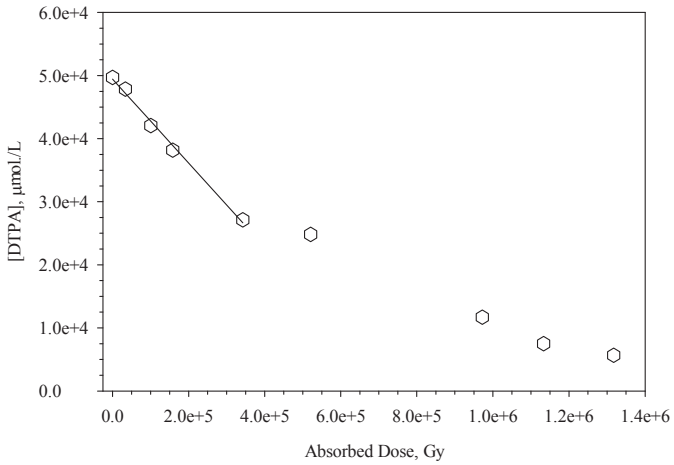

Figure 19. Concentration of DTPA determined by HPLC analysis as a function of absorbed dose for the static irradiation of aqueous TRUEX stripping reagent in contact with TRUEX solvent. The slope of the linear best-fit line corresponds to a *G*-value for the radiolytic degradation of DTPA of–G_{DTPA} = -0.067 ± 0.003 µmol·L^{-1}·Gy^{-1}. (R^2 = 0.99).

As was observed for the aqueous only static irradiation of the TRUEX stripping reagent, the static irradiation of the TRUEX stripping solution in contact with TRUEX solvent causes significant radiolytic degradation of lactic acid and DTPA. At the highest absorbed dose studied, the concentration of lactic acid has decreased by approximately 50 % and the DTPA concentration has decreased to nearly undetectable levels. The *G*-values for lactic acid degradation for the aqueous only and aqueous and organic static irradiations agree to within the experimental error (aqueous only: $-G_{\text{Lactic Acid}}$ = -0.617 ± 0.033 µmol·L^{-1}·Gy^{-1}; aqueous + organic: $-G_{\text{Lactic Acid}}$ = -0.583 ± 0.040 µmol·L^{-1}·Gy^{-1}). Since the hydroxyl radical ($^{\bullet}$OH) reacts rapidly with saturated aliphatic compounds, [4] the similarity of the LA *G*-values in the absence and presence of the aliphatic diluent suggests that $^{\bullet}$OH radical may not be solely responsible for the observed lactic acid degradation in the mixed phase system.

The organic solvent used for the static irradiations of the TRUEX aqueous and organic phases was analyzed in order to determine the variation in solvent composition as a function of absorbed dose. The variation in the concentration of CMPO as a function of absorbed dose present in the TRUEX solvent static irradiated in contact with the TRUEX aqueous strip solution is shown in Figure 20. The concentration of CMPO decreases sharply with increasing absorbed dose in an apparent exponential fashion. For non-linear (non-zero order) concentration versus dose plots, *G*-values are not an adequate metric with which to describe radiolytic yields.[13] However, despite their short-comings, initial *G*-values (G_0) have frequently been reported in the literature in this case, using the slope of the line asymptotic to the exponential. This results in a large *G*-value, $-G_{CMPO} = 0.527 \pm 0.108$ μmol·L^{-1}·Gy^{-1}, for the radiolytic degradation of CMPO is which, again, is too high to be explained by reaction by a simple bimolecular reaction. Chiarizia and Horwitz[14] used the decrease in extraction distribution ratio of Am to calculate $-G_{CMPO}$ = -0.55 μmol·L^{-1}·Gy^{-1} (ρ = 0.8 g/mL) for CMPO dissolved in decalin irradiated in contact with 5 M HNO_3. Nash et al. [15] reported $-G_{CMPO}$ ranging from 0.015 μmol·L^{-1}·Gy^{-1} (ρ = 0.8 g/mL) for TRUEX/dodecane up to 1.0 μmol·L^{-1}·Gy^{-1} (ρ = 1.6 g/mL) for CMPO/CCl_4 solutions γ-irradiated in contact with 5 M HNO_3.

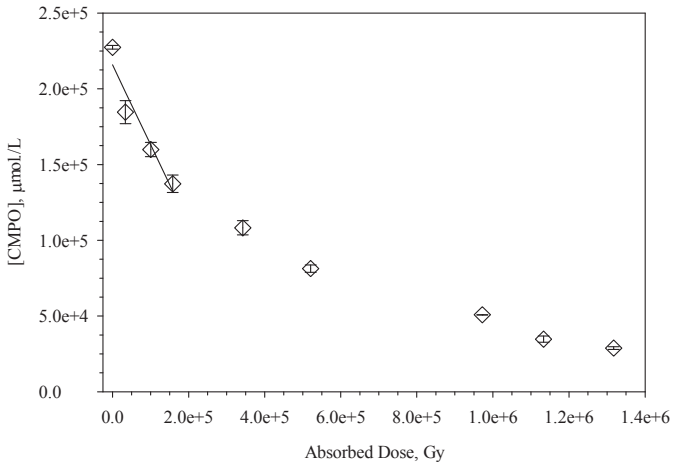

Figure 20. Concentration of CMPO present in the organic phase determined by HPLC analysis as a function of absorbed dose for the static irradiation of aqueous TRUEX stripping reagent in contact with TRUEX solvent. The slope of the linear best-fit line corresponds to a *G*-value for the radiolytic degradation of CMPO of $-G_{CMPO}$ = -0.527 ± 0.108 μmol·L^{-1}·Gy^{-1}. (R^2 = 0.88).

The variation in the concentration of TBP as a function of absorbed dose in the TRUEX solvent static irradiated in contact with the TRUEX aqueous strip solution is shown in Figure 21. Surprisingly, the *G*-value for the radiolytic degradation of TBP is significantly smaller than the value determined for CMPO degradation under the same conditions. This difference in *G*-values implies that TBP and CMPO follow different radiolytic degradation pathways under the conditions of the static radiolysis experiment.

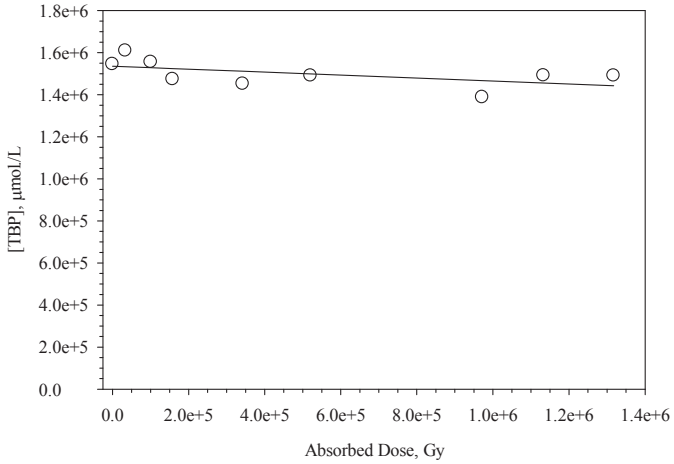

Figure 21. Concentration of TBP determined by GC-FID analysis as a function of absorbed dose for the static irradiation of aqueous TRUEX stripping reagent in contact with TRUEX solvent. The slope of the linear best-fit line corresponds to a *G*-value for the radiolytic degradation of TBP of $-G_{TBP} = -0.070 \pm 0.040$ μmol·L^{-1}·Gy^{-1}. (R^2 = 0.21).

Several products of the gamma radiolysis of TBP are easily identified and quantified. The main radiolysis product of TBP is dibutylphosphoric acid (HDBP). Some fraction of the HDBP that is formed via radiolysis of TBP may undergo further radiolysis to form monobutylphosphoric acid (H_2MBP).[1] The H_2MBP formed may undergo further reaction to form the phosphate anion. Additional TBP degradation products (mainly alcohols and organic esters) are present in these samples but the lack of suitable analytical standards impedes any meaningful quantification of these degradation products.

A plot of the concentration of HDBP present in the TRUEX solvent (determined by GC-FID analysis) static irradiated in contact with the aqueous TRUEX strip reagent as a function of absorbed dose is shown in Figure 22. The *G*-value for the formation of HDBP in the organic phase is $G_{HDBP} = 3.69 \times 10^{-3} \pm 1.43 \times 10^{-4}$ μmol·L^{-1}·Gy^{-1}. The concentration of HDBP formed in the TRUEX solvent increases linearly with increasing absorbed dose.

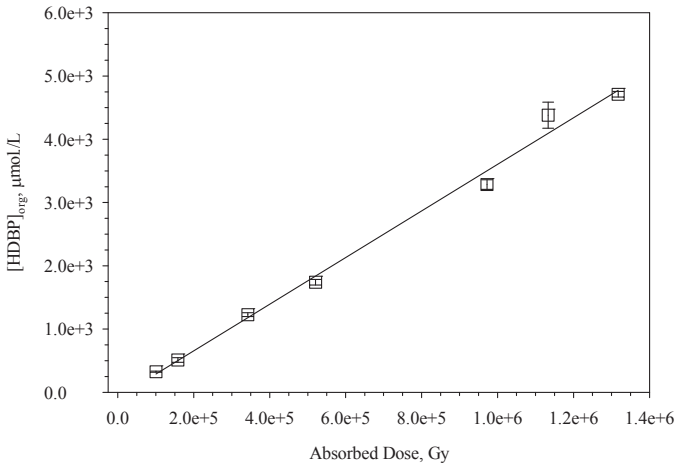

Figure 22. Concentration of HDBP present in the organic phase determined by GC-FID analysis as a function of absorbed dose for the static irradiation of aqueous TRUEX stripping reagent in contact with TRUEX solvent. The slope of the linear best-fit line corresponds to the *G*-value for the radiolytic production of HDBP in the organic phase of $G_{HDBP} = 3.69 \times 10^{-3} \pm 1.43 \times 10^{-4}$ µmol·L^{-1}·Gy^{-1}. ($R^2 = 0.99$).

Since HDBP exhibits some solubility in aqueous solution, some portion of the HDBP degradation product formed from the gamma radiolysis of TBP would be expected to partition to the aqueous phase. A plot of the concentration (determined by IC analysis) of HDBP present in the aqueous phase from static irradiation of TRUEX aqueous strip phase in contact with TRUEX solvent as a function of absorbed dose is shown in Figure 23. The *G*-value for the formation of HDBP in the aqueous phase is $2.47 \times 10^{-3} \pm 3.89 \times 10^{-4}$ µmol·L^{-1}·Gy^{-1}. The sum of these values leads to an over-all *G*-value for the radiolytic production of HDBP of $G_{HDBPtot} = 6.16 \times 10^{-3}$ µmol·L^{-1}·Gy^{-1}.

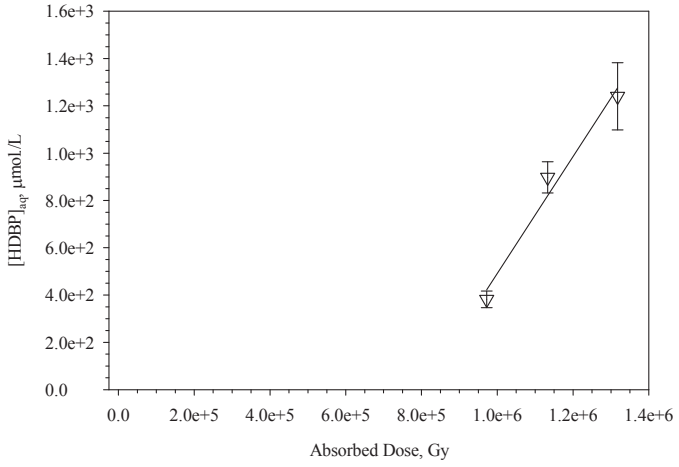

Figure 23. Concentration of HDBP present in the aqueous phase determined by IC analysis as a function of absorbed dose for the static irradiation of aqueous TRUEX stripping reagent in contact with TRUEX solvent. The slope of the linear best-fit line corresponds to a *G*-value for the radiolytic production of HDBP in aqueous phase of $G_{HDBP} = 2.47 \times 10^{-3} \pm 3.89 \times 10^{-4}$ µmol·L^{-1}·Gy^{-1}. ($R^2 = 0.95$).

Since HDBP is formed primarily by the degradation of TBP, the over-all *G*-value for HDBP formation is too low to account for the loss of TBP concentration in these samples. For example,

previously determined *G*-values for TBP degradation and HDBP formation for the test loop irradiation of TRUEX solvent in contact with a simple nitric acid aqueous phase [9] are, G_{TBP} = -0.114 μmol·L^{-1}·Gy^{-1} and G_{HDBP} = 0.118 μmol·L^{-1}·Gy^{-1}, respectively, indicating that essentially all the loss in TBP was accounted for by production of HDBP. Possible explanations for the low values determined for HDBP concentration in these samples in contact with the lactic acid/DTPA aqueous phase may be that the analytical technique is biased towards low HDBP concentrations or that some unidentified radiolysis reaction the degrades TBP to unidentified products other than HDBP or a process that consumes produced HDBP is occurring.

Grimes *et al.* [16] studied the partitioning of lactic acid to the organic phase in the TALSPEAK process. At an aqueous lactic acid concentration of 1.5 M, they determined $[LA]_{org}$ = 0.02 M. Since their study utilized the TALSPEAK solvent (0.2 M HDEHP in 1,4-diisopropylbenzene), the extent of lactic acid partitioning is not directly applicable to the current study. However, it is reasonable to assume that any lactic acid that does report to the TRUEX solvent may impact the HDBP analytical results by interfering with diazomethane used to derivatize the HDBP sample prior to GC analysis. Consumption of diazomethane by LA would result in apparently lower HDBP concentrations in the treated samples.

In order to determine the possible importance of LA interference with the GC analyses, the organic phases from the static irradiations of the TRUEX stripping section were analyzed by ion chromatography. An aliquot of the organic was contacted multiple times with water and the combined aqueous samples were analyzed. This IC analysis method did detect concentrations of HDBP in the organic samples approximately an order of magnitude smaller than the corresponding concentrations determined by the GC analyses. HDBP is only partially soluble in aqueous phases; so quantitative HDBP concentrations would not be obtained using this method. However, these results point to the conclusion that the GC HDBP analyses are likely not biased by the presence of lactic acid and represent the actual concentration of HDBP present in the samples. Therefore, the unexpectedly low HDBP concentrations are attributed to an unidentified radiolytic degradation process.

A plot of the concentration (determined by IC analysis) of H_2MBP present in the aqueous phase from static irradiation of TRUEX aqueous strip phase in contact with TRUEX solvent as a function of absorbed dose is shown in Figure 24. The *G*-value for the formation of H_2MBP in the aqueous phase is 5.22 x 10^{-4} ± 2.39 x 10^{-5} μmol·L^{-1}·Gy^{-1}.

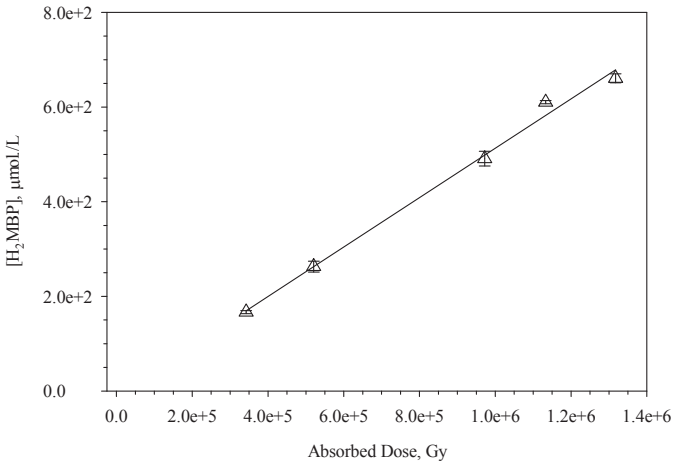

Figure 24. Concentration of H_2MBP present in the aqueous phase determined by IC analysis as a function of absorbed dose for the static irradiation of aqueous TRUEX stripping reagent in contact with TRUEX solvent. The slope of the linear best-fit line corresponds to a *G*-value for the radiolytic production of H_2MBP of $G_{H2MBP} = 5.22 \times 10^{-4} \pm 2.39 \times 10^{-5}$ µmol·L^{-1}·Gy^{-1}. ($R^2 = 0.99$).

A plot of the concentration (determined by IC analysis) of phosphate anion present in the aqueous phase from static irradiation of TRUEX aqueous strip phase in contact with TRUEX solvent as a function of absorbed dose is shown in Figure 25. The *G*-value for the formation of phosphate anion in the aqueous phase is $G_{Phos} = 1.16 \times 10^{-3} \pm 2.19 \times 10^{-4}$ µmol·L^{-1}·Gy^{-1}. The main source of phosphate anion in this system is expected to be monobutylphosphoric acid. A higher value of G_{Phos} compared to G_{H2MBP} would not appear to be consistent with H_2MBP being the source of phosphate anion. We have observed that H_2MBP is susceptible to hydrolysis in aqueous solution resulting in the formation of phosphate anion. This additional hydrolytic degradation would result in lower determined H_2MBP concentrations and a lower *G*-value for the production of H_2MBP than determined for the production of phosphate anion.

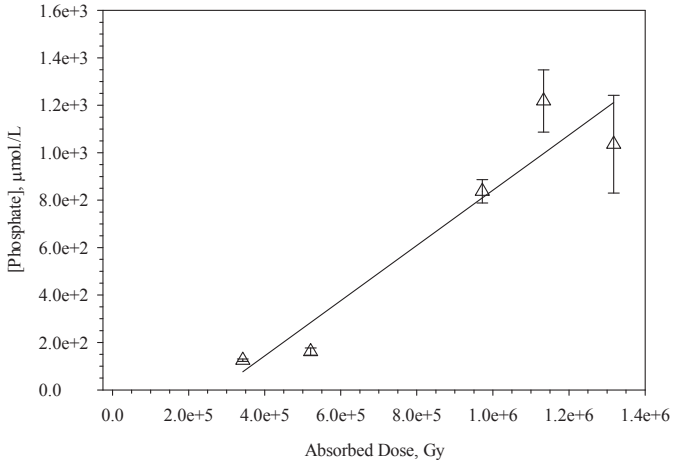

Figure 25. Concentration of phosphate anion present in the aqueous phase determined by IC analysis as a function of absorbed dose for the static irradiation of aqueous TRUEX stripping reagent in contact with TRUEX solvent. The slope of the linear best-fit line corresponds to a *G*-value for the radiolytic production of phosphate anion of $G_{Phos} = 1.16 \times 10^{-3} \pm 2.19 \times 10^{-4}$ µmol·L^{-1}·Gy^{-1}. ($R^2 = 0.99$).

The *G*-values determined for the static irradiation of the aqueous TRUEX strip reagent in contact with TRUEX solvent are summarized in Table 3.

Electrospray ionization mass spectrometry (ESI-MS) was used to attempt to identify the products formed in the aqueous phase by the static irradiation of the TRUEX aqueous strip solution in contact with TRUEX solvent. Only a summary of the ESI-MS results are presented. A detailed description of the ESI-MS results is available in the Appendix.

The positive ion spectrum of aqueous phase of un-irradiated sample contained significant ions derived from TBP (*m/z* 533, 267, 211, 155 and 99) and CMPO (*m/z* 408). Ions at *m/z* 394 and 416 are derived from DTPA, however these were at lower abundance. Ions originating from lactic acid were not intense, although they were present at *m/z* 91 $[(LA)H]^+$, 113 $[(LA)Na]^+$ and 135 $[(LA\text{-}H)Na_2]^+$. There were also ion signatures for the lactic acid ester at *m/z* 163 and 185, as previously identified. The high abundance of TBP-derived ions, and the lack of intense LA- or DTPA-derived ions is a consequence of the high sensitivity of ESI for TBP. TBP is a highly nucleophilic molecule as a result of its very high dipole moment, and at the same time is very surfacting, an attribute derived from its three hydrophobic butyl groups.

Table 3. *G*-values determined for the static irradiation of the aqueous TRUEX strip reagent in contact with TRUEX solvent.

Species	*G*-value, $\mu mol \cdot L^{-1} \cdot Gy^{-1}$	R^2
Lactic Acid	-0.585 ± 0.040	0.97
DTPA	$-6.65 \times 10^{-2} \pm 2.82 \times 10^{-3}$	0.99
CMPO	-0.527 ± 0.108	0.88
TBP	$-7.04 \times 10^{-2} \pm 3.96 \times 10^{-3}$	0.21
$HDBP_{org}$	$3.69 \times 10^{-3} \pm 1.43 \times 10^{-4}$	0.99
$HDBP_{aq}$	$2.47 \times 10^{-3} \pm 3.89 \times 10^{-4}$	0.95
$HDBP_{tot}$	6.16×10^{-3}	na
H_2MBP	$5.22 \times 10^{-4} \pm 2.39 \times 10^{-5}$	0.99
Phosphate	$1.16 \times 10^{-3} \pm 2.19 \times 10^{-4}$	0.87

At an absorbed dose of 342 kGy, the ion spectrum contained largely the same suite of ions, although the DTPA-derived ions were reduced in intensity. A new ion at *m/z* 172 is hypothesized to be protonated dibutyl,propylammonium $[(iBu)_2NPrH]^+$, an assignment consistent with the MS^2 spectrum which shows the elimination of C_4H_8 to form *m/z* 116. The ion at *m/z* 130 is the dibutyl ammonium cation $[(iBu)_2NH_2]^+$. Both of these amine ions have been observed in previous studies of CMPO degradation by direct infusion ESI[17] and GC analysis of irradiated organic solutions.[15, 18]

The samples from the highest absorbed dose experiments (up to 1032 kGy) contained ions from HDBP, for which ESI also has a high sensitivity. The two protonated amine degradation products at *m/z* 130 and *m/z* 172, which arise from CMPO degradation, are present in abundance, as are unidentified product ions at *m/z* 260 and 118. In addition, ions corresponding to $[(iBu)_2NH_2]^+$ and CMPO-caroxylic acid are observed. Ions derived from intact lactic acid, DTPA, and CMPO are in very low abundance in the spectra of the high dose samples, indicating that they have undergone nearly complete radiolytic degradation.

Plots of ion intensities as a function of absorbed dose for ions derived from LA, DTPA, DTPA lactam, CMPO, and CMPO degradation products are presented in Figures 26 – 30, respectively. The variations of the intensities with absorbed dose for the ions corresponding to LA, DTPA, and DTPA

lactam for the static irradiation of the aqueous and organic mixtures are very similar to the ion intensities observed for the irradiation of the aqueous TRUEX strip solution. The absence of a significant variation in ion intensity for ions corresponding to CMPO degradation products at absorbed doses greater than 342 kGy (see Figure 30) suggests that the CMPO degradation products are subject to further radiolytic degradation.

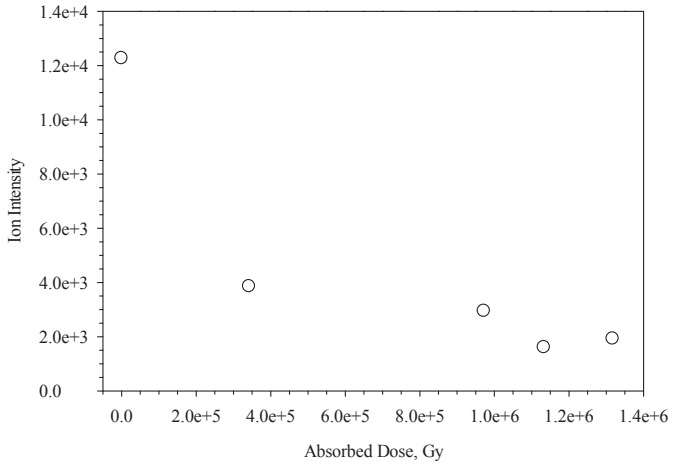

Figure 26. Positive ion intensity versus absorbed dose corresponding to ions derived from LA and lactic acid esters for the static irradiation of the TRUEX aqueous strip solution in contact with TRUEX solvent.

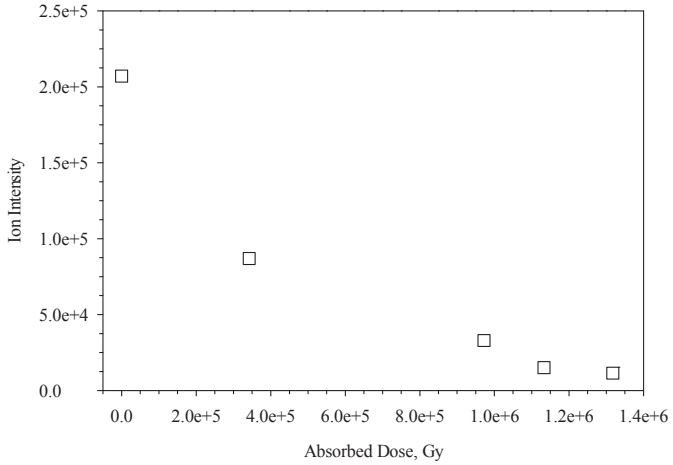

Figure 27. Positive ion intensity versus absorbed dose corresponding to ions derived from DTPA for the static irradiation of the TRUEX aqueous strip solution in contact with TRUEX solvent.

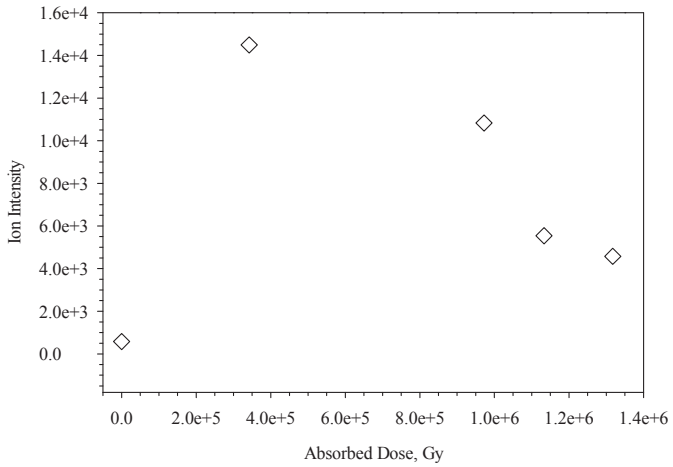

Figure 28. Positive ion intensity versus absorbed dose corresponding to ions derived from DTPA lactam for the static irradiation of the TRUEX aqueous strip solution in contact with TRUEX solvent.

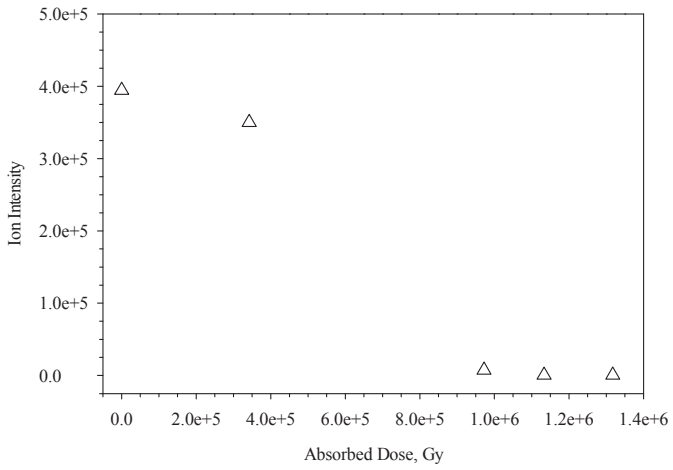

Figure 29. Positive ion intensity versus absorbed dose corresponding to ions derived from CMPO for the static irradiation of the TRUEX aqueous strip solution in contact with TRUEX solvent.

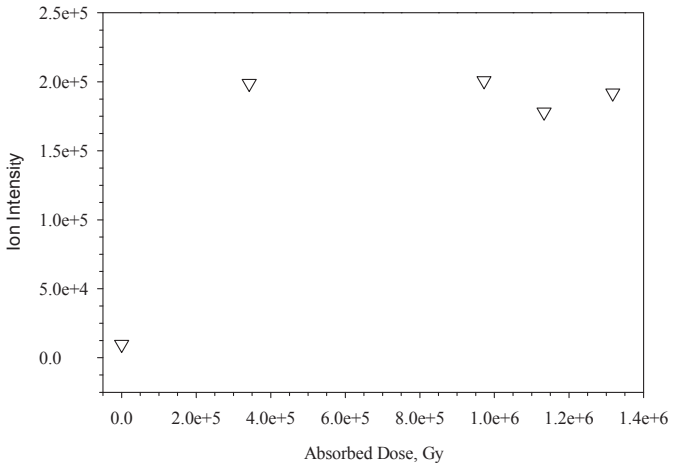

Figure 30. Positive ion intensity versus absorbed dose corresponding to ions derived from CMPO degradation products for the static irradiation of the TRUEX aqueous strip solution in contact with TRUEX solvent.

The negative ion ESI analysis of aqueous phases from the static irradiation of the aqueous and organic mixture of the TRUEX stripping system revealed similar results for LA and DTPA. The pyruvic acid degradation products indentified for the aqueous only irradiations were also present in the mixed phase static irradiations. CMPO and its degradation products were not readily detected in the negative ion ESI analysis. Interestingly, the ion intensity corresponding to HDBP formed by the radiolytic degradation of TBP appears to increase with increasing absorbed dose (see Figure 31). This increase would seem to conflict with the assertion that an unidentified degradation process consumes HBDP; accounting for the unexpectedly low value of G_{HDBP} determined in this work. However, this trend may, also, be attributed to the very high sensitivity of ESI for organophosphorous compounds. Clearly, further studies will be necessary to satisfactorily explain the apparently anomalous degradation behavior of HDBP occurring in the TRUEX stripping section.

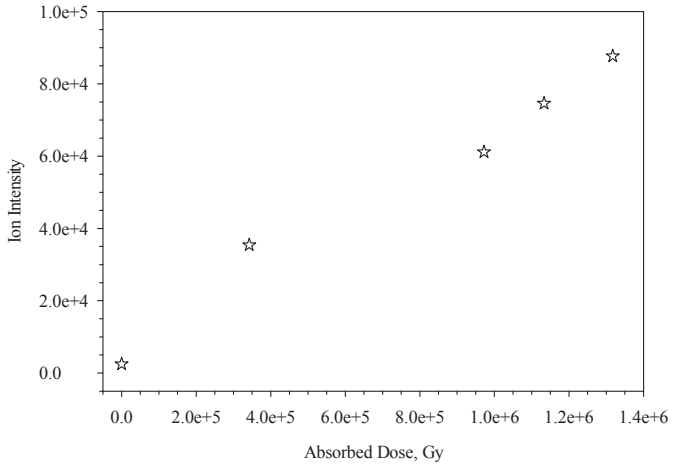

Figure 31. Negative ion intensity versus absorbed dose corresponding to HDBP present in the aqueous phase of the static irradiation of the TRUEX aqueous strip solution in contact with TRUEX solvent.

3.4 Test Loop Irradiation of Strip Section of TRUEX Flowsheet

The TRUEX stripping solution was irradiated in the INL radiolysis test loop while in contact with TRUEX solvent. These irradiations were conducted with the test loop operating under an ambient atmosphere, i.e. all solutions were exposed to atmospheric oxygen. This approach more closely approximates the processing conditions that an actual solvent extraction system would experience.

The concentration of lactic acid determined by IC analysis as a function of absorbed dose for the test loop irradiation of the mixed phase is shown in Figure 32. The lactic acid concentration determined at 0 kGy absorbed dose is approximately 13% higher than the nominal concentration. Since little variation in the lactic acid concentration with increasing absorbed dose is observed, the 0 kGy concentration is considered to be erroneous and not used in the *G*-value determination for lactic acid. The *G*-value for the radiolytic degradation of lactic acid in the test loop is $G_{\text{Lactic acid}}$ = -5.15 x 10^{-2} μmol·L^{-1}·Gy^{-1}. This *G*-value for lactic acid degradation is approximately an order of magnitude smaller than determined from the static irradiation experiments (see Figures 10 and 18, Tables 2 and 3). This difference probably indicates that a reactive species is being scavenged by oxygen which results in less lactic acid degradation.

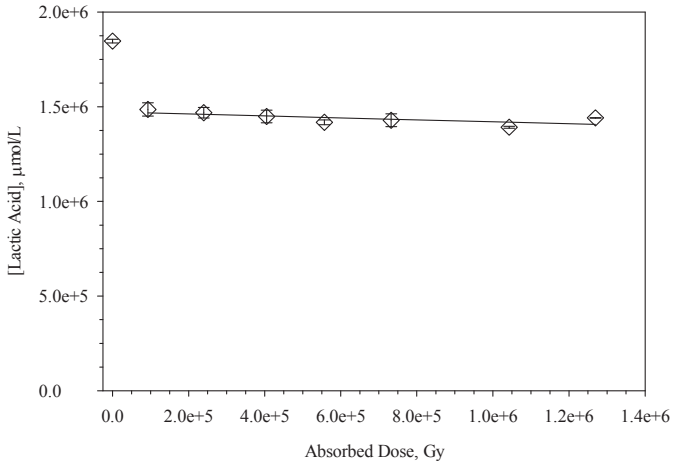

Figure 32. Concentration of lactic acid determined by IC analysis as a function of absorbed dose for the test loop irradiation of aqueous TRUEX stripping reagent in contact with TRUEX solvent. The slope of the linear best-fit line corresponds to a *G*-value for the radiolytic degradation of lactic acid of $-G_{LA}$ = -5.18 x 10^{-2} ± 2.36 x 10^{-2} μmol·L^{-1}·Gy^{-1}. (R^2 = 0.39).

The concentration of DTPA determined by HPLC analysis as a function of absorbed dose for the test loop irradiation of TRUEX stripping reagent and TRUEX solvent is shown in Figure 33. The *G*-value for the degradation of DTPA is G_{DTPA} = -4.75 x 10^{-2} ± 9.45 x 10^{-3} μmol·L^{-1}·Gy^{-1}. Similar *G*-values for DTPA degradation were determined for all the radiolysis conditions examined in this work. In all studied cases, irradiation of the TRUEX stripping reagent to absorbed doses on the order of 1000 kGy or higher leads to essentially complete radiolytic degradation of DTPA.

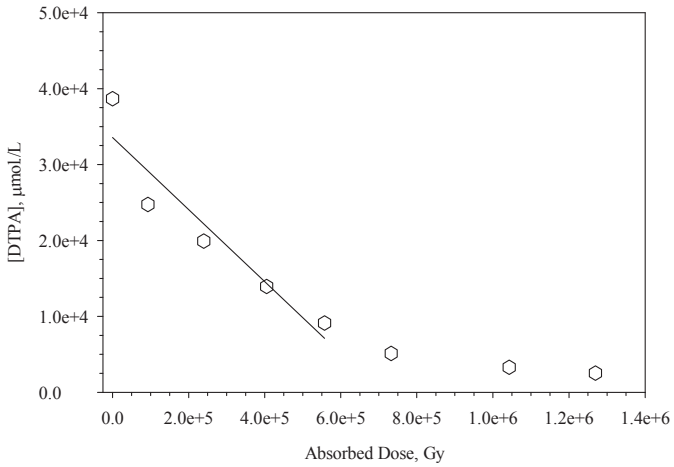

Figure 33. Concentration of DTPA determined by HPLC analysis as a function of absorbed dose for the test loop irradiation of aqueous TRUEX stripping reagent in contact with TRUEX solvent. The slope of the linear best-fit line corresponds to a *G*-value for the radiolytic degradation of DTPA of $-G_{DTPA}$ = -4.75 x 10^{-2} ± 9.45 x 10^{-3} µmol·L^{-1}·Gy^{-1}. (R^2 = 0.86).

The HPLC procedure used to determine DTPA in the aqueous phase detected several degradation products. The concentration of radiolytically-produced acetate as a function of absorbed dose for the test loop irradiation of the TRUEX stripping section is plotted in Figure 34. The *G*-value for the production of acetate is $G_{Acetate}$ = 1.20 x 10^{-2} µmol·L^{-1}·Gy^{-1}. The acetate degradation product could result from the cleavage of a C-N bond within DTPA. Toste et al.[19] studied the gamma radiolysis of ethylenediaminetetraacetic acid (EDTA) in simulated Hanford Site waste and reported formation of numerous carboxylic and dicarboxylic acids. Unfortunately, the authors did not report *G*-values in their work. Since EDTA and DTPA are both polyaminopolycarboxylic acids, the production of acetate from DTPA radiolysis seems reasonable.

The remaining degradation products identified by the HPLC analysis of the aqueous samples from the test loop irradiated TRUEX stripping section are shown in Figures 35 and 36. Since these products are unknowns, no *G*-values for their production can be determined. Attempts to identify these degradation products and the degradation product co-eluting with DTPA at high absorbed dose (see Figure 9) by HPLC-ESI were not successful.

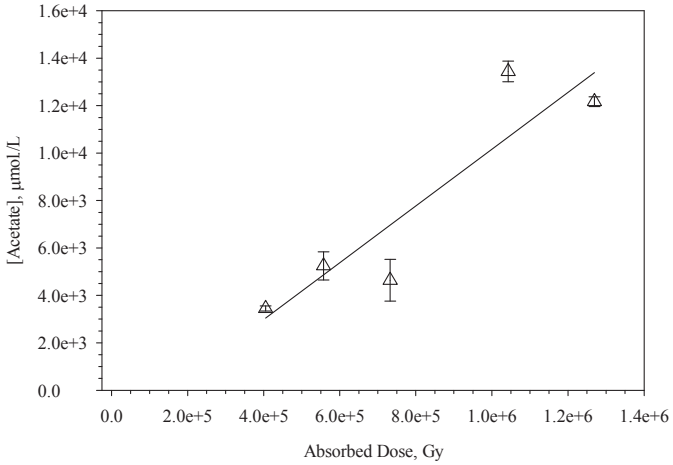

Figure 34. Concentration of acetate determined in the aqueous phase by HPLC analysis as a function of absorbed dose for the test loop irradiation of aqueous TRUEX stripping reagent in contact with TRUEX solvent. The slope of the linear best-fit line corresponds to a *G*-value for the radiolytic production of acetate of $G_{Acetate}$ = 1.20 x 10^{-2} ± 3.15 x 10^{-3} µmol·L^{-1}·Gy^{-1}. (R^2 = 0.77).

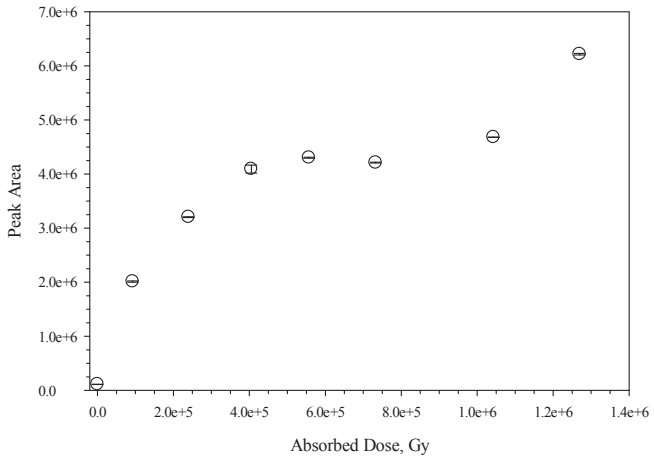

Figure 35. Plot of the peak area versus absorbed dose corresponding to an aqueous soluble degradation product (HPLC retention time: 3.4 min) formed during the test loop irradiation of aqueous TRUEX stripping reagent in contact with TRUEX solvent.

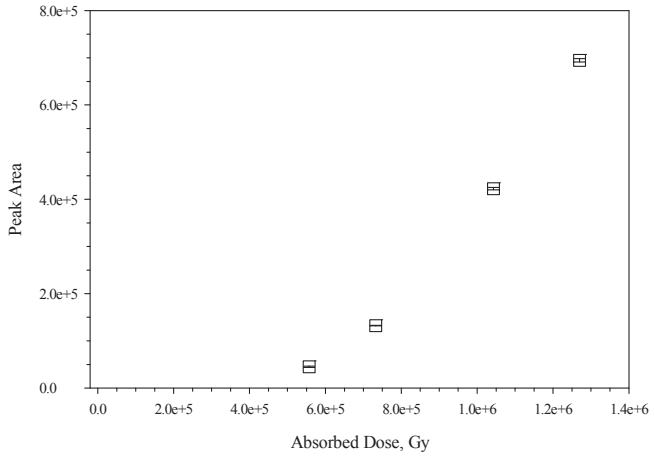

Figure 36. Plot of the peak area versus absorbed dose corresponding to an aqueous soluble degradation product (HPLC retention time: 6.7 min) formed during the test loop irradiation of aqueous TRUEX stripping reagent in contact with TRUEX solvent.

The decrease in the concentration of CMPO in the test loop for the irradiated mixed phase is shown as a function of absorbed dose in Figure 37. While the concentration of CMPO decreases with increasing absorbed dose, the decrease in concentration is significantly less than observed for static irradiation of the TRUEX strip section (see Figure 21). For the test loop, the *G*-value for the radiolytic degradation of CMPO, G_{CMPO} = -3.67 x 10^{-2} ± 5.07 x 10^{-3} μmol·L^{-1}·Gy^{-1} indicates, again, the oxygen present in the test loop is scavenging a reactive species resulting in less CMPO degradation compared to the extent of degradation observed in the static irradiations.

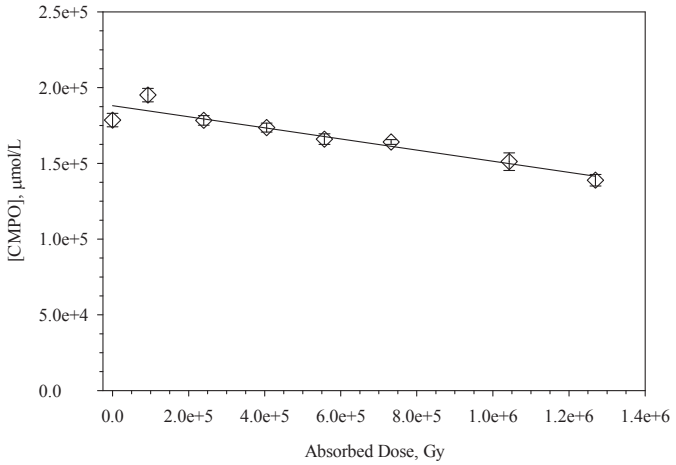

Figure 37. Concentration of CMPO present in the organic phase determined by HPLC analysis as a function of absorbed dose for the test loop irradiation of aqueous TRUEX stripping reagent in contact with TRUEX solvent. The slope of the linear best-fit line corresponds to a *G*-value for the radiolytic degradation of CMPO of $-G_{CMPO}$ = -3.67 x 10^{-2} ± 5.07 x 10^{-3} μmol·L^{-1}·Gy^{-1}. (R^2 = 0.88).

The primary difference between the conditions of the static and test loop irradiations is the presence of oxygen in the test loop. While oxygen is present in the samples subjected to static irradiations, radiolytic degradation of any oxygen initially present is complete after an absorbed dose of ~0.5 kGy is achieved.[20] The actual mechanism by which dissolved oxygen present in the test loop ameliorates the radiolytic degradation is not known. However, the rapid reaction of oxygen with carbon centered radicals generated from diluent radiolysis would produce less reactive peroxyl radicals.[2] These peroxyl radicals decay to form stable products. Further studies are necessary in order to develop a complete understanding of the inhibition of radiolytic degradation of CMPO in the presence of oxygen.

The decrease in the concentration of TBP present in the test loop irradiated TRUEX strip section as function of absorbed dose is shown in Figure 38. The *G*-value for the radiolytic degradation of TBP in the test loop is G_{TBP} = -3.00 x 10^{-2} ± 1.54 x 10^{-2} μmol·L^{-1}·Gy^{-1}. The smaller value of G_{TBP} for the test loop irradiation again indicates that the organic solvent is less susceptible to radiolytic degradation when irradiated using the test loop conditions.

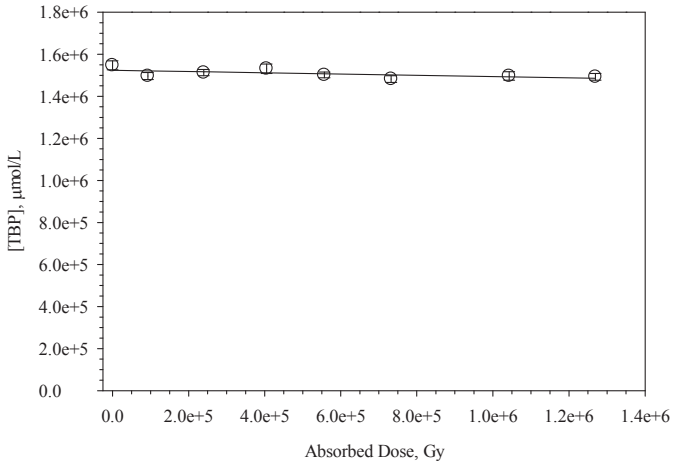

Figure 38. Concentration of TBP determined by GC-FID analysis as a function of absorbed dose for the test loop irradiation of aqueous TRUEX stripping reagent in contact with TRUEX solvent. The slope of the linear best-fit line corresponds to a *G*-value for the radiolytic degradation of TBP of $-G_{TBP}$ = -3.00 x 10^{-2} ± 1.54 x 10^{-2} μmol·L^{-1}·Gy^{-1}. (R^2 = 0.29).

The organic phase concentration of HDBP produced via the radiolytic degradation of TBP in the test loop irradiated TRUEX strip section as function of absorbed dose is shown in Figure 39. The *G*-value for the radiolytic production of HDBP in the test loop is G_{HDBP} = 4.29 x 10^{-3} ± 3.46 x 10^{-4} μmol·L^{-1}·Gy^{-1}. The concentration of HDBP increases linearly in absorbed dose. A plot of the concentration (determined by IC analysis) of HDBP present in the aqueous phase from the test loop irradiation of the TRUEX stripping section as a function of absorbed dose is shown in Figure 40. The *G*-value for the formation of HDBP in the aqueous phase is 1.96 x 10^{-3} ± 3.73 x 10^{-4} μmol·L^{-1}·Gy^{-1}.

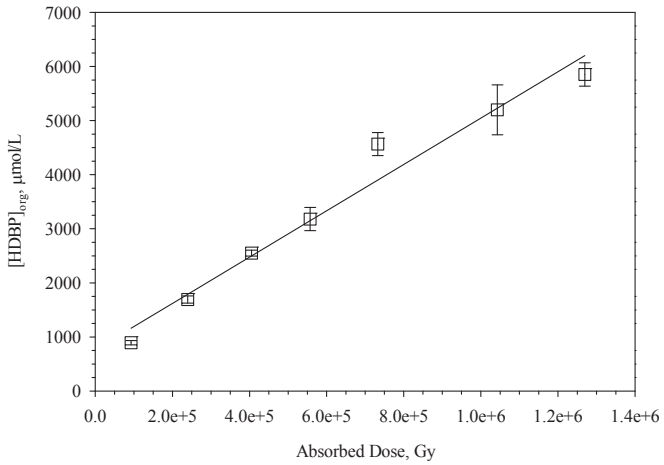

Figure 39. Concentration of HDBP present in the organic phase determined by GC-FID analysis as a function of absorbed dose for the test loop irradiation of aqueous TRUEX stripping reagent in contact with TRUEX solvent. The slope of the linear best-fit line corresponds to a *G*-value for the radiolytic production of HDBP in the organic phase of $G_{HDBP} = 4.29 \times 10^{-3} \pm 3.46 \times 10^{-4}$ µmol·L^{-1}·Gy^{-1}. ($R^2 = 0.96$).

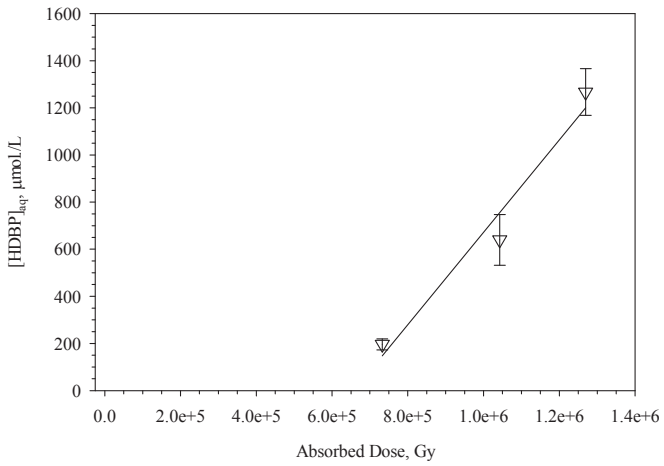

Figure 40. Concentration of HDBP present in the aqueous phase determined by IC analysis as a function of absorbed dose for the test loop irradiation of aqueous TRUEX stripping reagent in contact with TRUEX solvent. The slope of the linear best-fit line corresponds to a *G*-value for the radiolytic production of HDBP in aqueous phase of $G_{HDBP} = 1.96 \times 10^{-3} \pm 3.73 \times 10^{-4}$ µmol·L^{-1}·Gy^{-1}. ($R^2 = 0.93$).

The sum of these values leads to an over-all *G*-value for the radiolytic production of HDBP of $G_{HDBPtot} = 6.25 \times 10^{-3}$ µmol·L^{-1}·Gy^{-1}. As was observed in the case of the static irradiations of the TRUEX stripping section, this value is lower than would be expected based upon the *G*-value determined for TBP radiolytic degradation, $G_{TBP} = -3.00 \times 10^{-2}$ µmol·L^{-1}·Gy^{-1}. An unidentified process appears to be responsible for the degradation of HDBP which results from the radiolysis of TBP, for irradiation in the presence of this lactic acid/DTPA aqueous phase.

A plot of the concentration of H_2MBP present in the aqueous phase from test loop irradiation of TRUEX stripping section as a function of absorbed dose is shown in Figure 41. The *G*-value for the formation of H_2MBP in the aqueous phase is $4.39 \times 10^{-4} \pm 1.06 \times 10^{-5}$ μmol·L^{-1}·Gy^{-1}.

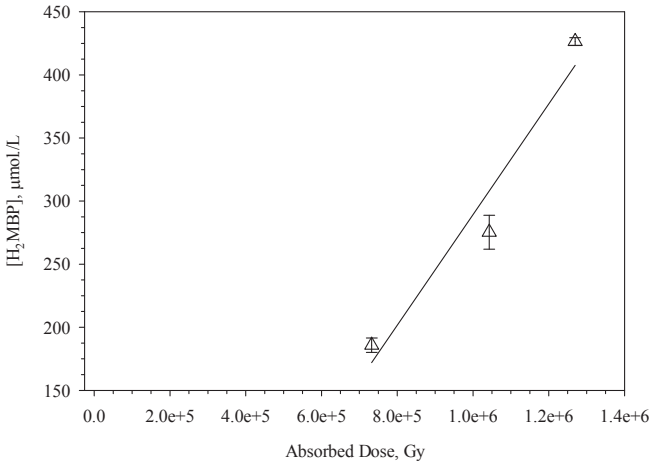

Figure 41. Concentration of H_2MBP present in the aqueous phase determined by IC analysis as a function of absorbed dose for the test loop irradiation of aqueous TRUEX stripping reagent in contact with TRUEX solvent. The slope of the linear best-fit line corresponds to a *G*-value for the radiolytic prodution of H_2MBP of $G_{H2MBP} = 4.39 \times 10^{-4} \pm 1.06 \times 10^{-5}$ μmol·L^{-1}·Gy^{-1}. ($R^2 = 0.89$).

A plot of the concentration of phosphate anion present in the aqueous phase from static irradiation of TRUEX aqueous strip phase in contact with TRUEX solvent as a function of absorbed dose is shown in Figure 42. The *G*-value for the formation of phosphate anion in the aqueous phase is $G_{Phos} = 8.15 \times 10^{-4} \pm 1.36 \times 10^{-4}$ μmol·L^{-1}·Gy^{-1}. The main source of phosphate anion in this system is expected to be monobutylphosphoric acid. As was observed for the static irradiations, a higher value of G_{Phos} than G_{H2MBP} was determined. Again, this discrepancy is attributed to further degradation of H_2MBP by hydrolysis which forms additional phosphate anion.

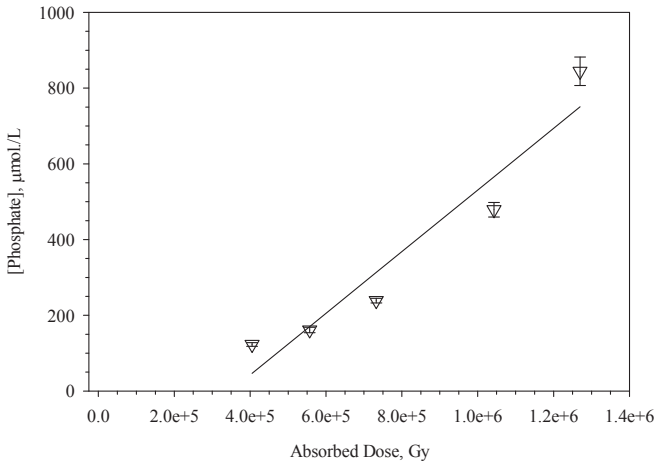

Figure 42. Concentration of phosphate anion present in the aqueous phase determined by IC analysis as a function of absorbed dose for the static irradiation of aqueous TRUEX stripping reagent in contact with TRUEX solvent. The slope of the linear best-fit line corresponds to a *G*-value for the radiolytic production of phosphate anion of $G_{Phos} = 1.16 \times 10^{-3} \pm 2.19 \times 10^{-4}$ µmol·L^{-1}·Gy^{-1}. ($R^2 = 0.99$).

Electrospray ionization mass spectrometry (ESI-MS) was used to attempt identify the products formed in the aqueous phase by the test loop irradiation of the TRUEX aqueous strip solution in contact with TRUEX solvent. Only a summary of the ESI-MS results are presented. A detailed description of the ESI-MS results is available in the Appendix.

The positive ion ESI analysis of the aqueous phase corresponding to the un-irradiated test loop sample displayed intense ions derived from the lactate esters and DTPA. Similar results were seen for the zero absorbed dose sample static irradiation analyses. The positive ion analysis of the 405 kGy absorbed dose sample contained abundant signals derived from TBP, which shows up as the protonated molecule at *m/z* 267 $[(TBP)H]^+$. Under ESI conditions, $[(TBP)H]^+$ undergoes elimination of 1, 2, and 3 C_4H_8 molecules forming *m/z* 211, 155 and 99, respectively. In addition, TBP in the test loop undergoes elimination of C_4H_8, forming DBP and MBP, and these also produce ion signals at *m/z* 211, 155 and 99. At higher radiation doses, these ion signals are augmented, while that of intact TBP is less intense, signaling clearly that TBP radiolysis is occurring.

The mass spectrum of the 733 kGy absorbed dose sample (Figure A-1a) was very similar to that absorbed at 405 kGy absorbed dose. At these high absorbed doses, there was no longer any indication of intact DTPA or CMPO, however ions derived from the DTPA lactam and CMPO degradation products were observed. Changes in the spectrum of the 1040 kGy absorbed dose sample were observed, namely an increase in the intensity of HDBP-derived ions. At the highest absorbed dose studied (1270 kGy), ions attributable to TBP and HDBP were still observed albeit at lower abundance. There was no longer any indication of intact DTPA or CMPO, however ion derived from the DTPA lactam and CMPO degradation products were observed.

Plots of ion intensities as a function of absorbed dose for ions derived from LA, DTPA, DTPA lactam, CMPO degradation products, and TBP are presented in Figures 43 - 47, respectively.

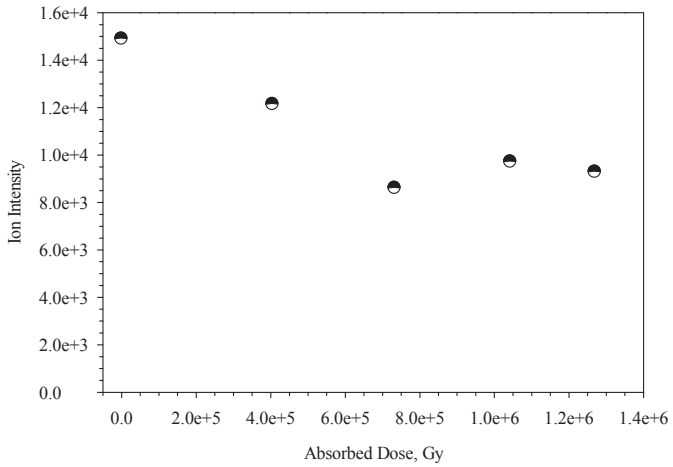

Figure 43. Positive ion intensity versus absorbed dose corresponding to ions derived from LA and lactic acid esters for the test loop irradiation of the TRUEX aqueous strip solution in contact with TRUEX solvent.

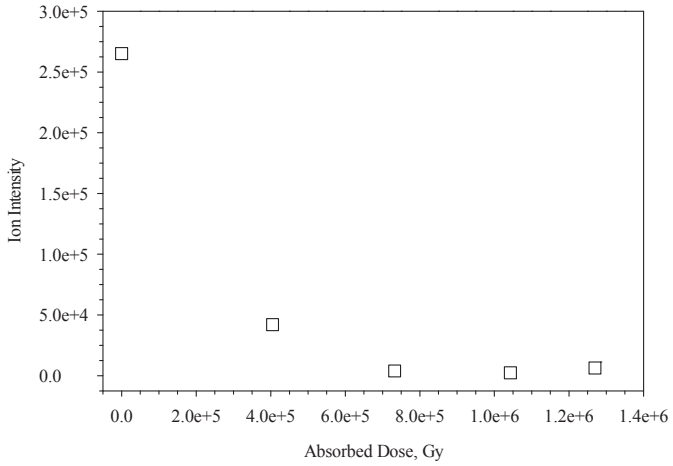

Figure 44. Positive ion intensity versus absorbed dose corresponding to ions derived from DTPA for the test loop irradiation of the TRUEX aqueous strip solution in contact with TRUEX solvent.

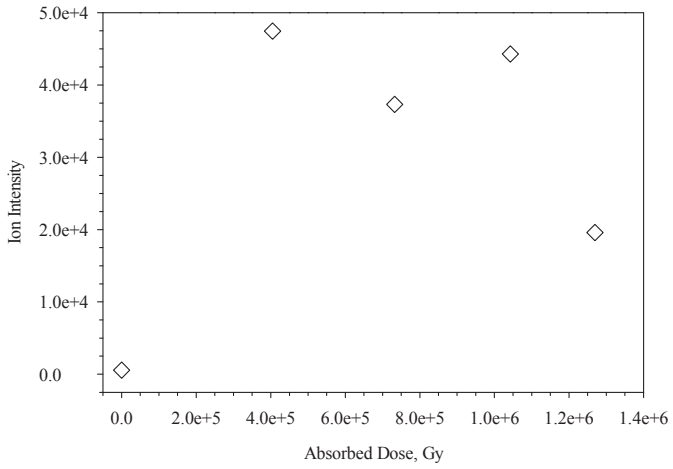

Figure 45. Positive ion intensity versus absorbed dose corresponding to ions derived from the DTPA lactam degradation product for the test loop irradiation of the TRUEX aqueous strip solution in contact with TRUEX solvent.

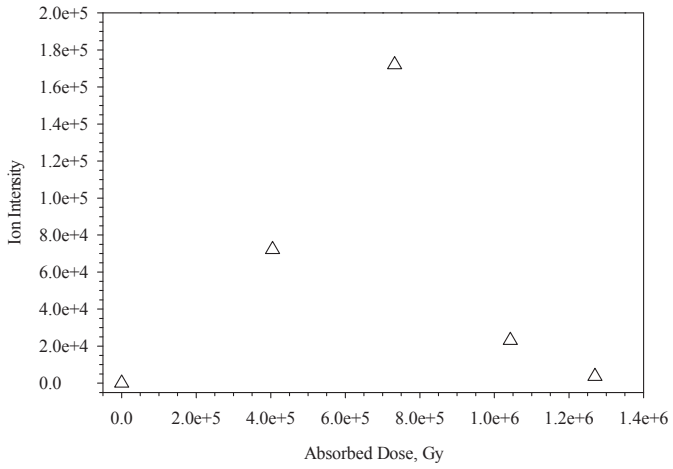

Figure 46. Positive ion intensity versus absorbed dose corresponding to ions derived from the products of CMPO degradation for the test loop irradiation of the TRUEX aqueous strip solution in contact with TRUEX solvent.

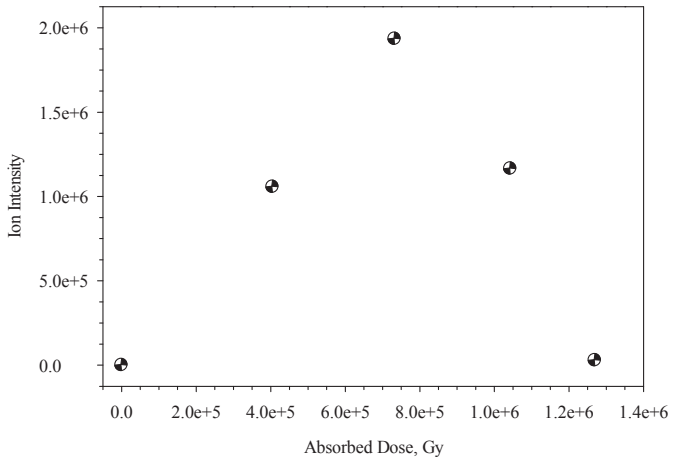

Figure 47. Positive ion intensity versus absorbed dose corresponding to ions derived from TBP for the test loop irradiation of the TRUEX aqueous strip solution in contact with TRUEX solvent.

The anion ESI analysis of the zero absorbed dose test loop sample showed an abundant ion at *m/z* 89 that corresponds to the lactic acid conjugate base $[LA\text{-}H]^-$. Other ions in the spectrum correspond to the lactic acid self esterification reaction, or clusters of this and lactic acid. In addition to products derived from LA, ions derived from DTPA were observed, highlighted by the conjugate base at *m/z* 392. In addition natiated versions were seen at *m/z* 414 and 436, which are formed by Na-for-H substitution in the ESI droplets. These ions confirm the DTPA assignments positive ion analysis, being 2 mass units lower (two protons, switching the polarity from positive to negative).

The anion ESI mass spectrum of the 405 kGy absorbed sample contained abundant ions derived from DBP, notably the conjugate base at *m/z* 209, and cluster ions with lactate and the lactate ester at *m/z* 321 and 393. Ions corresponding to intact DTPA are still seen, albeit at lower abundance, and the DTPA-lactam conjugate base is now observed at *m/z* 316. These ions are complementary to the cations seen for this compound at *m/z* 318 and 340, and further confirm the existence of a degradation product having a molecular weight of 317 g/mol, that we hypothesize to be the DTPA lactam.

The anion spectra of samples which received 733, 1040, and 1270 kGy absorbed doses are very similar, containing the same ions noted above for the 405 kGy sample with the salient exception that the DTPA conjugate base is gone. This no doubt signals complete radiolysis of DTPA by the dose corresponding to 733 kGy. The ions derived from the DTPA lactam are still present, although they appear decreased in abundance compared to the 405 kGy sample; this suggests that the lactam undergoes further radiolytic degradation however we have not yet determined what it becomes.

The *G*-values determined for the test loop irradiation of the aqueous TRUEX strip reagent in contact with TRUEX solvent are summarized in Table 4. The *G*-values determined for test loop irradiation of TRUEX in contact with 4.4 M HNO_3 [10, 21] are summarized Table 5. Comparison of the *G*-values determined for these irradiation conditions indicate that degradation due to radiolysis occurs via differing processes in these systems.

Table 4. *G*-values determined for the test loop irradiation of the aqueous TRUEX strip reagent in contact with TRUEX solvent.

Species	*G*-value, $\mu mol \cdot L^{-1} \cdot Gy^{-1}$	R^2
Lactic Acid	$-5.18 \times 10^{-2} \pm 2.37 \times 10^{-2}$	0.39
DTPA	$-4.75 \times 10^{-2} \pm 9.46 \times 10^{-3}$	0.86
Acetate	$1.20 \times 10^{-2} \pm 3.15 \times 10^{-3}$	0.77
CMPO	$-3.67 \times 10^{-2} \pm 5.07 \times 10^{-3}$	0.88
TBP	$-3.00 \times 10^{-2} \pm 1.06 \times 10^{-4}$	0.29
$HDBP_{org}$	$4.29 \times 10^{-3} \pm 3.46 \times 10^{-4}$	0.96
$HDBP_{aq}$	$1.96 \times 10^{-3} \pm 3.73 \times 10^{-4}$	0.93
$HDBP_{tot}$	6.25×10^{-3}	Na
H_2MBP	$4.39 \times 10^{-4} \pm 1.06 \times 10^{-5}$	0.89
Phosphate	$8.15 \times 10^{-4} \pm 1.37 \times 10^{-4}$	0.90

Table 5. Summary of *G*-values determined for the test loop irradiation of TRUEX solvent in contact with 4.4 M HNO_3.

Species	*G*-value, $\mu mol \cdot L^{-1} \cdot Gy^{-1}$	R^2
TBP	-0.115 ± 0.031	0.62
CMPO	-0.159 ± 0.016	0.97
$HDBP_{tot}$	0.118 ± 0.007	0.97
H_2MBP	$1.56 \times 10^{-3} \pm 8.06 \times 10^{-5}$	0.99
Phosphate	$5.66 \times 10^{-3} \pm 3.94 \times 10^{-4}$	0.98

Gamma radiolysis results in a small increase the distribution ratios in the strip section of the TRUEX flowsheet (D_{Am} = <0.001 at 0 kGy absorbed dose to D_{Am} = 0.015 at 1300 kGy absorbed). Even the distribution ratio determined for the highest absorbed dose is not expected to adversely impact operation of the stripping section of the TRUEX flowsheet. However, the generation of degradation products in the aqueous phase and the radiolytic destruction of lactic acid and DTPA may have serious impacts on a subsequent TALSPEAK process. Close coupling of the TRUEX and TALSPEAK operations may help to mitigate these effects by limiting the dose to the aqueous and subsequent degradation.

4. Conclusions

The effects of gamma radiolysis upon the efficacy of the strip section of a TRUEX flowsheet for the recovery of trivalent actinides and lanthanides from acidic solution were determined by a combination of static and test loop irradiations. Compositions of the irradiated aqueous and organic solutions were

determined using a suite of analytical techniques. In addition, ESI-MS was used to identify some of the products of the radiolytic degradation of lactic acid, DTPA, CMPO, and TBP.

For lactic acid, the major degradation products detected by ESI-MS were pyruvic acid and a species corresponding to a lactic acid-pyruvic acid cluster. The major product of DTPA degradation was determined by ESI-MS to be a DTPA lactam resulting from the radiolytic loss of glycolic acid. Acetate and several other unknown degradation products of both lactic acid and DTPA were detected by HPLC analysis. Several species arising from the degradation of CMPO ($[(iBu)_2NPrH]^+$, $[(iBu)_2PrH_2]^+$ and CMPO-carboxylic acids) were determined by ESI-MS; which is consistent products identified in previous studies.

Comparison of the test loop irradiations of the TRUEX extraction and stripping sections revealed surprising differences in the radiolytic degradation of TBP and HDBP. Based upon our results, an unidentified process is responsible for the degradation of HDBP which results from the radiolysis of TBP, for irradiation in the presence of lactic acid/DTPA aqueous phase. Further study would be necessary to develop a detailed understanding the radiation chemistry of TBP and HDBP in contact with a lactic acid/DTPA aqueous solution.

The generally lower *G*-values determined for test loop irradiation compared to static irradiation experiments clearly points out the importance of performing radiolytic degradation studies using oxygenated, mixed aqueous and organic solutions. The actual mechanism by which dissolved oxygen present in the test loop ameliorates the radiolytic degradation is not known. However, the rapid reaction of oxygen with carbon centered radicals would produce less reactive peroxyl radicals. Further studies are necessary in order to develop a complete understanding of the role played by dissolved oxygen in the inhibition of radiolytic degradation of solvent extraction process solvents.

Gamma radiolysis results in a small increase the distribution ratios in the strip section of the TRUEX flowsheet (D_{Am} = <0.001 at 0 kGy absorbed dose to D_{Am} = 0.015 at 1300 kGy absorbed). Even the distribution ratio determined for the highest absorbed dose is not expected to adversely impact operation of the stripping section of the TRUEX flowsheet. However, the generation of degradation products in the aqueous phase and the radiolytic destruction of lactic acid and DTPA may have serious impacts on a subsequent TALSPEAK process. Close coupling of the TRUEX and TALSPEAK operations may help to mitigate these effects by limiting the gamma dose to the strip product solution.

5. Acknowledgements

The authors thank Bruce J. Mincher for the many useful discussions of radiation chemistry in aqueous and organic solutions. The authors, also, thank William F. Bauer for assistance with the completion of the HPLC analysis of DTPA.

6. References

1. Mincher, B.J.; Modolo, G.; Mezyk, S.P. The Effects of Radiation Chemistry on Solvent Extraction: 1. Conditions in Acidic Solution and a Review of TBP Radiolysis. *Solv.Extr. Ion Exch.* **2009,** *27*, 1- 25.

2. Mincher, B.J.; Mezyk, S.P. Radiation chemcial effects on radiochemistry: A review of examples important to nuclear power. *Radiochimica Acta* **2009,** *97*, 519-534.

3. Mincher, B.; Modolo, G.; Mezyk, S. The Effects of Radiation Chemistry on Solvent Extraction 3 : A Review of Actinide and Lanthanide Extraction. *Solv. Extr. Ion Exch.* **2009,** *27*, 579-606.

4. Buxton, G.V.; Greenstock, C.L.; Helman, W.P.; Ross, A.B. Critical review of rate constants for reactions of hydrated electrons, hydrogen atoms and hydroxyl radicals ($\cdot OH/\cdot O^-$) in aqueous solution. *J. Phys. Chem. Ref. Data* **1988,** *17*, 513-886.

5. Sehested, K. The Fricke Dosimeter. In *Manual on Radiation Dosimetry*; Holm, N.W.; Berry, R.J. Eds. Marcel Dekker, Inc, New York, 1970; pp. 313-317.

6. Ajji, Z. Usability of aqueous solutions of mehtyl red as high-dose dosimeter for gamma radiation. *Radiat. Meas.* **2006,** *41*, 438-442.

7. Black, T.H. The preparation and reactions of diazomethane. *Aldrichimica Acta* **1983,** *16*, 3-10.

8. Dodi, A.; Verda, G. Improved determination of tributyl phosphate degradation products (mono- and dibutyl phosphates) by ion chromatography *J. Chrom. A* **2001,** *920*, 275-281.

9. Peterman, D.R.; Olson, L.G.; McDowell, R.G.; Elias, G.; Law, J.D. *Summary of TRUEX Radiolysis Testing Using the INL Radiolysis Test Loop.* FCRD-SWF-2012-000082, Idaho National Laboratory: Idaho Falls, ID, 2012.

10. Peterman, D.R.; Olson, L.G.; Tillotson, R.D.; McDowell, R.G.; Law, J.D. *TRUEX Radiolysis Testing Using the INL Radiolysis Test Loop: FY-2012 Status Report*. FCRD-SWF-2012-000303, Idaho National Laboratory: Idaho Falls, ID. 2012.

11. Bibler, N.E., Gamma and alpha radiolysis of aqueous solutions of diethylenetriaminepentaacetic acid. *J. Inorg.Nuc. Chem.* **1972,** *34*, 1417-1425.

12. Hobel, B.; von Sonntag, C., OH-Radical induced degradation of ethylenediaminetetraacetic acid (EDTA) in aqueous solution: a pulse radiolysis study. *J. Chem. Soc., Perkin Trans. 2* **1998,** 509-514.

13. Mincher, B.J.; Curry, R.D., Considerations for choice of a kinetic fig. of merit in process radiation chemistry for waste treatment. *Appl. Radiat. Iso.* **2000,** *52*, 189-193.

14. Chiarizia, R.; Horwitz, E.P., Hydrolytic and radiolytic degradation of octyl(phenyl)-N-N-diisobutylcarbamoylmethylphosphine oxide and related compounds. *Solv. Extr. Ion Exch.* **1986,** *4*, 677-723.

15. Nash, K.L.; Rickert, P.G.; Horwitz, E.P. Degradation of TRUEX-Dodecane Process Solvent. *Solv. Extr. Ion Exch.***1989,** *7*, 655-675.

16. Grimes, T.S.; Nilsson, M.A.; Nash, K.L. Lactic acid partitioning in TALSPEAK extraction systems. *Sep. Sci. Technol.* **2010,** *45*, 1725-1732.

17. Groenewold, G.S.; Elias, G.; Mincher, B.J.; Mezyk, S.P.; LaVerne, J.A. Characterization of CMPO and its radiolysis products by direct infusion ESI-MS. *Talanta* **2012,** *99*, 909-917.

18. Nash, K.L.; Gatrone, R.C.; Clark, G.A.; Rickert, P.G.; Horwitz, E.P. Hydrolytic and Radiolytic Degradation of OÏ†d(iB)Cmpo: Continuing Studies. *Sep. Sci. Technol.* **1988,** *23*, 1355-1372.

19. Toste, A.P.; Polach, K.J.; Ohnuki, T. Fuel cycle and nuclear waste. *J. Radioanal. Nuc. Chem.* **2005,** *263*, 559-565.

20. Spinks, J.W.T.; Woods, R.J. In *An Introduction to Radiation Chemistry*; John Wiley & Sons: New York, 1964 p. 270.

21. Peterman, D.R.; McDowell, R.G.; Olson, L.G.; Tillotson, R.D. *FY-2011 Status Report for the Radiolysis and Hydrolysis Test Loop.* FCRD-SWF-2011-000286, Idaho National Laboratory: Idaho Falls, ID, 2011.

22. Martin, L.R.; Mezyk, S.P.; Mincher, B.J., Determination of Arrhenius and Thermodynamic Parameters for the Aqueous Reaction of the Hydroxyl Radical with Lactic Acid. *J. Phys. Chem. A* **2008,** *113*, 141-145.

SEPARATION AND WASTEFORMS CAMPAIGN

7. Appendix A "Summary of ESI-MS Analyses of Irradiated TRUEX Strip Samples"

Summary of ESI-MS Analyses of Irradiated TRUEX Strip Samples

Static Irradiation TRUEX Aqueous Strip: TS series

A total of six samples were provided designated: TS0, TS4, TS7, TS8 and TS9. The samples had not been contacted with the organic layer. Stripping solutions containing 1.5 M lactic acid and 50 mM DTPA were diluted 1:250 using a 9:1 H_2O:MeOH solution (identical to the test loop solutions).
Positive Ion Analyses

The cation spectrum of sample TS0 contained only low abundance ions corresponding to intact lactic acid in the form of $[(LA)Na]^+$ and $[(LA\text{-}H)Na_2]^+$ at *m/z* 113 and 135. Instead, abundant ions at *m/z* 185 and 257 were observed (Figure A-1, Table 1), that correspond to the esterified derivatives of LA (as seen in the test loop samples). These ions were natiated, and further incorporation of Na was seen as ions at *m/z* 273 and 207. In addition to the natiated esters, ammoniated esters were seen at *m/z* 180 and 252; the origin of the ammonium is undetermined at this point, but MS^2 of these ions results in elimination of 17 u, indicative of elimination of NH_3, and consistent with molecules cationized by NH_4^+. Part of the reason for the low abundance of the lactic acid derived ions is that LA is clustering with the esters, which accounts for ions at *m/z* 345, 369 and 391 in Figure A-1a.

Table A-1. Compositions and origins of cations seen in the ESI mass spectra of the non-contact samples.

m/z	Composition	Compound derived from	Absorbed Dose, kGy
185	[(LA ester)Na]+	LA	0.0
252	[(LA diester)NH4]+	LA	0.0
257	[(LA diester)Na]+	LA	0.0
273	[(LA ester)(pyruvic acid)Na]+	LA, pyruvate	914 - 1530
279	[(LA diester-H)Na2]+	LA	0.0
318	[(DTPA lactam)H]+	DTPA	393
340	[(DTPA lactam)Na]+	DTPA	393
347	[(LA diester)(LA)Na]+	LA	0.0
369	$[(LA\text{ diester-H})(LA)Na_2]^+$	LA	0.0
391	$[(LA\text{ diester-H})(LA\text{-H})Na_3]^+$	LA	0.0

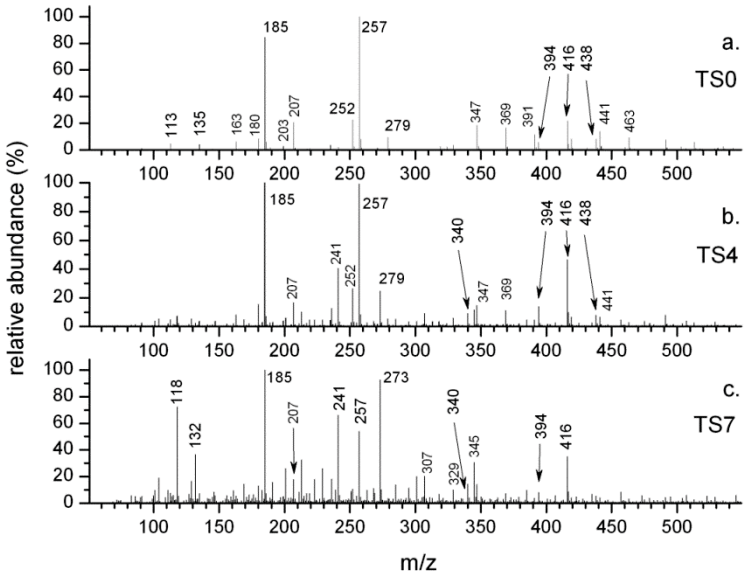

Figure A-1. Cation ESI mass spectra of the non-contacted samples TS0, TS4 and TS7.

Two new ions are observed at *m/z* 318 and 340 that are unequivocally derived from DTPA degradation; this conclusion is supported by accurate *m/z* measurements, which are consistent with the proposed elemental composition (see below), and by collision induced dissociation (CID) reactions. The fact that the two ions are separated by 22 u indicates that *m/z* 318 is protonated, while *m/z* 340 is natiated. Thus the molecular weight of the degradation product is 317 g/mol, representing a loss of 76 g/mol compared to DTPA. We hypothesize that this corresponds to the radiolytic loss of glycolic acid, forming a lactam product (Figure A-2). The protonated lactam at *m/z* 318 undergoes CID to *m/z* 185, which corresponds to the loss of 133 amu, or $HN(CH_2CO_2H)_2$, formed by cleavage of the pendant amine (Figure A-3). The CID behavior of protonated DTPA is similar, but cleaving at the central amine, eliminating 161 amu to form *m/z* 233.

Cation analyses of more heavily irradiated samples TS7, TS8 and TS9 produced similar spectra; that became more complex with increasing dose (Figure A-4). Several trends could be observed, notably that DTPA-derived ions (e.g. *m/z* 416) continued to decrease in intensity as dose increased, as did the LA ester-derived ions (*m/z* 185 and 257). Ions at *m/z* 273, 132 and 118 increased; the former is hypothesized to be a cluster ion formed form the LA ester and pyruvic acid, i.e. $[(\text{LA ester})(\text{pyruvic acid})\text{Na}]^+$. A similar rationale can be used for *m/z* 345, which is hypothesized to be $[(\text{LA diester})(\text{pyruvic acid})\text{Na}]^+$. The participation of pyruvic acid in the cluster formation chemistry is consistent with the anion analyses, which showed strong evidence for pyruvate. The ions at *m/z* 118 and 132 do not have satisfactory explanations at this time; however they will have elemental compositions containing one N atom (on the basis of formation of even electron species). Their accurate *m/z* values are consistent with compositions of $C_6H_{16}NO^+$ and $C_7H_{18}NO^+$, which could correspond to hydroxyl amine compounds, however, the origin of such compounds has not been satisfactorily hypothesized to date.

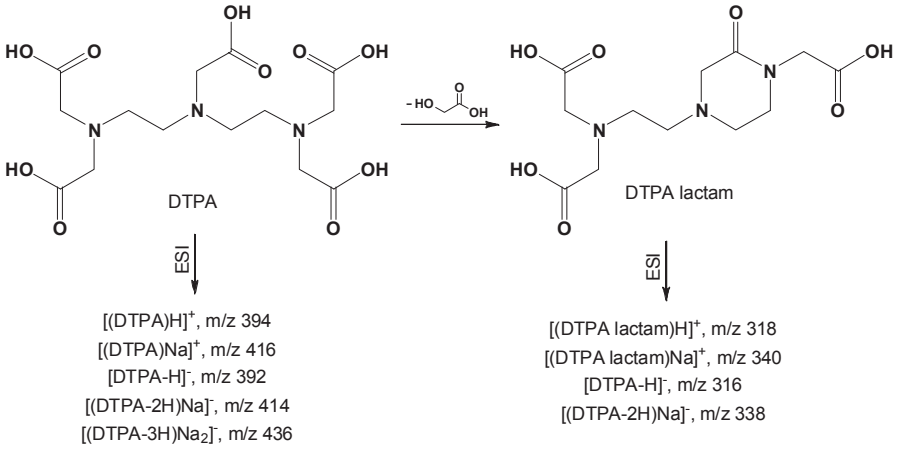

Figure A-2. Radiolytic degradation of DTPA to form the DTPA lactam, and the CID elimination supporting the assignment.

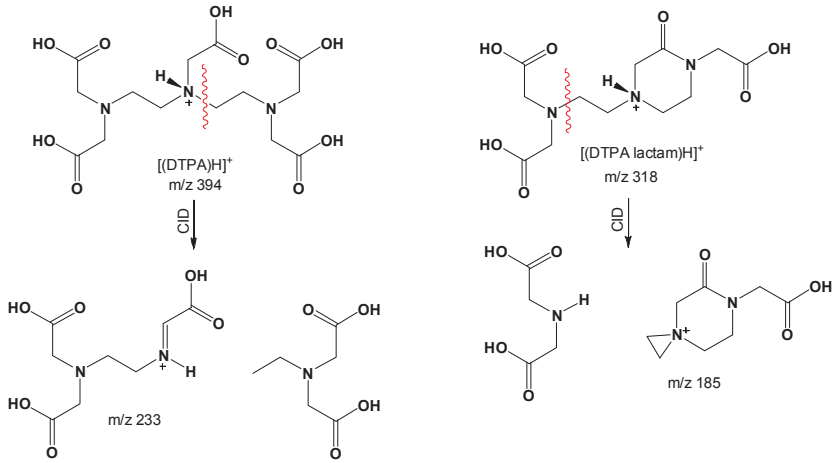

Figure A-3. CID reactions of [(DTPA)H]+ and [(DTPA lactam)H]+.

The cation infusion profiles of the DTPA-derived ions decreased as dose increased, i.e. from TS0 through TS9 (see Figure A-4). The DTPA-derived ions summed for this analysis were [(DTPA)H]+ at *m/z* 394, and the natiated DTPA ions at *m/z* 416, 438, 460 and 482. The decrease in the DTPA-derived ions was not as dramatic as in the case of the test loop samples, which suggested that the other compounds in the test loop may in fact increase the rate of DTPA degradation. Degradation of DTPA was accompanied by the appearance of the DTPA lactam, which showed up as the protonated and natiated molecules in the mass spectra at *m/z* 318 and 340; these were summed to produce the DTPA lactam profile. The DTPA lactam derived ions decrease in the samples receiving the highest doses, indicating that the DTPA lactam was undergoing additional degradation reactions.

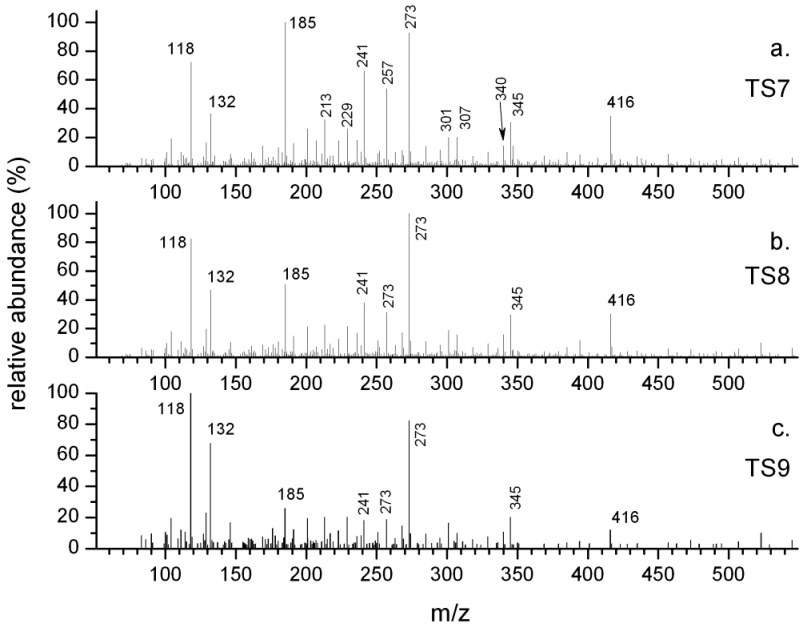

Figure A-4. Positive ion ESI mass spectra of noncontacted samples TS7, TS8 and TS9.

The numerical average intensities for the positive ions resulting from lactic acid in the static irradiation of the TRUEX strip aqueous phase are summarized in Table A-2. The numerical average intensities for the ions resulting from lactic acid esters are summarized in Table A-3. The numerical average intensities for the ions resulting from DTPA are summarized in Table A-4. The numerical average intensities for the ions resulting from the DTPA lactam degradation product are summarized in Table A-5.

Table A-2. Numerical averages for the cations derived from lactic acid as a function of absorbed dose for the static irradiation of the TRUEX aqueous strip solution.

Absorbed Dose, kGy	*m/z* 91	*m/z* 113	*m/z* 135	sum LA
	[(LA)H]+	[(LA)Na]+	[(LA-H)Na]+	
0.0	1781	8652	7404	17837
393	2180	4537	3540	10257
914	1785	2673	2540	6998
1170	2109	1226	1267	4602
1530	1870	0	0	1870

Table A-3. Numerical averages for the cations derived from lactic acid esters as a function of absorbed dose for the static irradiation of the TRUEX aqueous strip solution.

Absorbed Dose, kGy	*m/z* 163	*m/z* 185	*m/z* 207	*m/z* 235	*m/z* 257	sum LA diester
	[(La ester)H]+	[(LA ester)Na]+	[(LA ester-H)Na2]+	[(La diester)H]+	[(LA diester)Na]+	
0.0	11190	159422	38574	6502	188556	212620
393	7586	94825	15890	4070	94245	103393
914	1923	35422	6270	1039	19131	21413
1170	1925	21506	3182	1379	13192	16120
1530	1380	12628	2674	1832	9183	12694

Table A-4. Numerical averages for the cations derived from DTPA as a function of absorbed dose for the static irradiation of the TRUEX aqueous strip solution.

Absorbed Dose, kGy	*m/z* 394	*m/z* 416	*m/z* 438	sum DTPA
	[(DTPA)H]+	[(DTPA)Na]+	[(DTPA-H)Na2]+	
0.0	10335	40627	14994	65956
393	13186	44187	7528	64901
914	2826	12353	1864	17043
1170	5052	12804	1344	19200
1530	2281	5832	0	8113

Table A-5. Numerical averages for the cations derived from DTPA lactam degradation product as a function of absorbed dose for the static irradiation of the TRUEX aqueous strip solution.

Absorbed Dose, kGy	*m/z* 318	*m/z* 340	sum DTPA lactam
	[(DTPA lactam)H]+	[(DTPA lactam)Na]+	
0.0	0	113	113
393	3089	8718	11807
914	2393	5045	7438
1170	2996	6778	9774
1530	2882	5236	8118

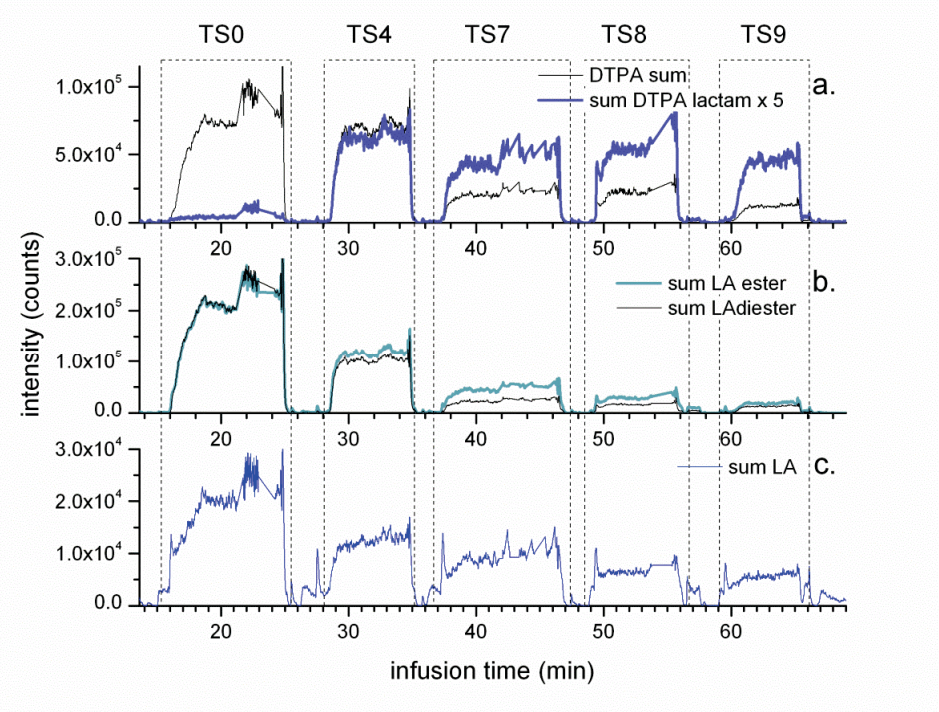

Figure A-4. Infusion profiles, non-contacted samples TS0, TS4, TS7, TS8 and TS9. The DTPA sum was generated from *m/z*394, 416, 438 and 460. The DTPA lactam sum was generated from *m/z* 318 and 340. The LA ester sum was generated from *m/z* 163, 185 and 207. The LA diester sum was generated from *m/z* 235, 257 and 273. The LA sum was generated from *m/z* 91, 113 and 135.

Non-Contacted Samples, Negative Ion Analyses

Analysis of the TS 0 sample showed an abundant $[DTPA-H]^-$ at *m/z* 392, together with an abundant $[LA-H]^-$ at *m/z* 89 (Figure A-5). A low abundance ion at *m/z* 161 is attributed to the conjugate base of the lactic acid ester. The signal at *m/z* 187 has't been identified, but undergoes CID dissociation by loss of 72 u to *m/z* 115, suggesting that it is another lactate ester derivative. The negative ESI mass spectrum of the first irradiated sample TS4 displays $[LA-H]^-$, $[(LA\ ester)-H]^-$ and $[DTPA-H]^-$ at *m/z* 89, 161 and 392, respectively, but also contains a significant ion at *m/z* 177 (Figure c). CID of this ion shows fragmentation to *m/z* 89 and 87, suggesting that it is a proton-bound dimer of lactate and pyruvate. Pyruvic acid has a molecular weight of 88 g/mol, with a corresponding conjugate base having a *m/z* value of 87. Pyruvate has vicinal carbonyl groups, which would make it a strongly complexing ligand. We hypothesize that pyruvate is formed from radiolysis of lactate. Low abundance ions at *m/z* 321 and 249 also suggest lactate ester – lactate – pyruvate clusters, as indicated by their CID spectra. Significantly, the conjugate base of the DTPA lactam is seen at *m/z* 316 at low abundance, indicating radiolysis of DTPA.

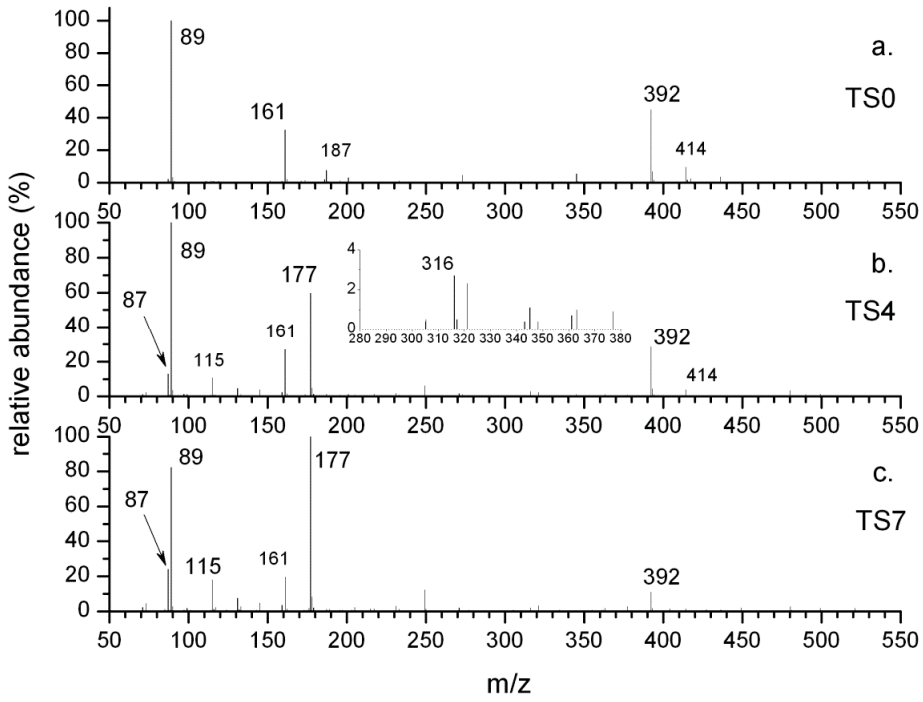

Figure A-5. Anion ESI mass spectra of the non-contacted samples TS0, TS4 and TS7.

The anion mass spectra of samples TS7, TS8 and TS9 (see Figure A-6) are largely identical to that of TS4. There are systematic changes in the relative abundances of $[LA\text{-}H]^-$ (*m/z* 89), $[DTPA\text{-}H]^-$ (*m/z* 392), pyruvate (*m/z* 87) and the putative lactate-pyruvate cluster ion (177). Both $[LA\text{-}H]^-$ and $[DTPA\text{-}H]^-$ steadily decrease in abundance with increasing dose, i.e., from TS4 to TS9. In contrast, the pyruvate containing ions *m/z* 87 and 177 steadily increase. This suggests that LA and DTPA are undergoing radiolysis, while pyruvate is being formed. A product ion at *m/z* 115 builds in with increasing dose, but has not been identified.

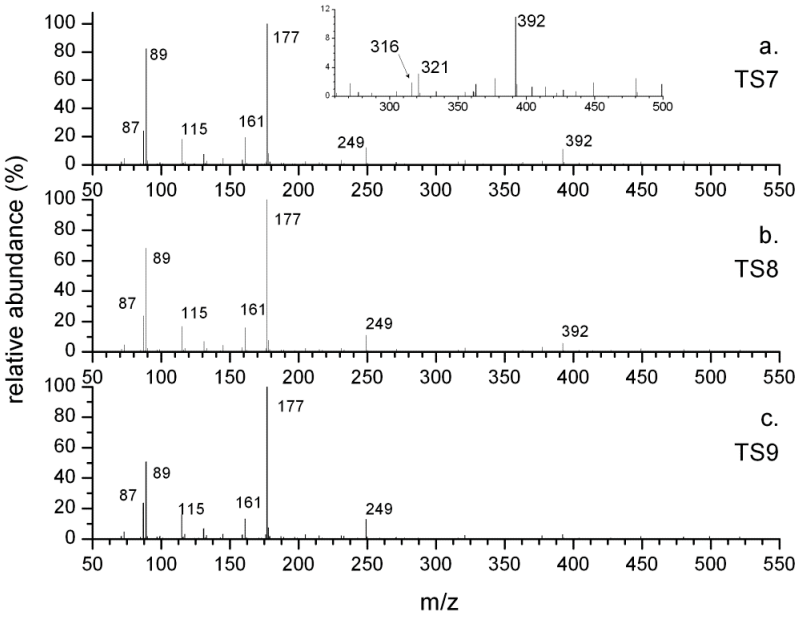

Figure A-6. Anion ESI mass spectra of the non-contacted samples TS7, TS8, and TS9.

The trends are more easily observed in the infusion profiles for the five samples (see Figure A-7). The ions corresponding to the conjugate bases of LA and the LA ester are seen to steadily decrease with increasing sample number and dose. At the same time pyruvate and the pyruvate cluster (*m/z* 87 and 177) steadily increase, suggesting that pyruvate comes from lactate. Finally, the DTPA conjugate base at *m/z* 392 decreases steadily, while the conjugate base of the DTPA lactam initially rises and then falls again, suggesting that it is formed from DTPA by radiolysis, but then undergoes subsequent radiolysis reactions.

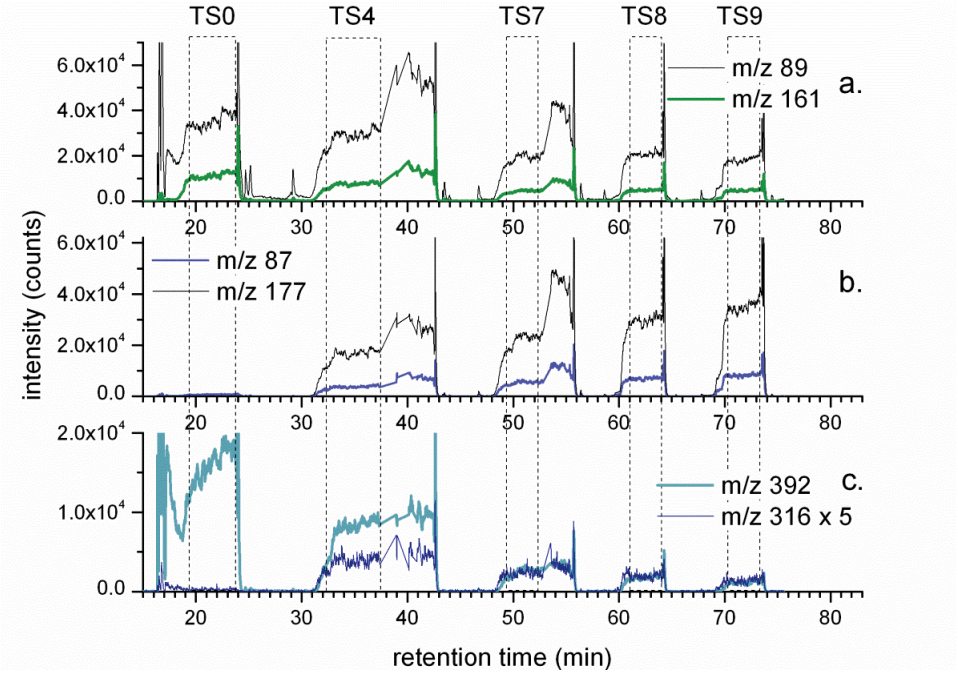

Figure A-7. Infusion profiles for anions derived from lactate, pyruvate, lactate ester, DTPA and DTPA lactam, TS series sample analyses.

The numerical average intensities for the negative ions resulting from lactic acid, DTPA, and degradation products formed in the static irradiation of the TRUEX strip aqueous phase are summarized in Table A- 6.

Table 6. Numerical averages for the important anions in the ESI analyses of the TS series samples.

sample	Absorbed Dose, kGy	*m/z* 87	*m/z* 89	*m/z* 161	*m/z* 177	*m/z* 316	*m/z* 392
		pyruvate	lactate	lactate ester	LA-PA cluster	DTPA lactam	DTPA
TS0	0.0	666	33281	10740	101	34	14914
TS4	393	2190	28268	7570	16814	751	8039
TS7	914	5564	19036	4500	23130	441	2538
TS8	1170	6938	19950	4682	29300	342	1649
TS9	1530	8185	17555	4616	34645	243	1001

Analysis of Organic-Contacted Strip Solutions (TOS series)

Stripping solutions containing 1.5 M lactic acid and 50 mM DTPA that had been contacted with the TBP/CMPO-bearing organic phase were diluted 1:250 using a 9:1 H2O:MeOH solution (as in the case of the test loop solutions and the non-contacted solutions).

Positive ion direct infusion studies

The positive ion spectrum of unirradiated sample TOS 0 contained significant ions derived from TBP (*m/z* 533, 267, 211, 155 and 99) and CMPO (*m/z* 408) (see Figure A-9). Ions at *m/z* 394 and 416 are derived from DTPA, however these were at lower abundance. Ions originating from lactic acid were not intense, although they were present at *m/z* 91 $[(LA)H]^+$, 113 $[(LA)Na]^+$ and 135 $[(LA\text{-}H)Na_2]^+$. There were also ion signatures for the lactic acid ester at *m/z* 163 and 185, as previously identified.

The lowest irradiated sample TOS 4 contained largely the same suite of ions, although the DTPA-derived ions were reduced in intensity. *M/z* 172 is hypothesized to be protonated dibutyl,propylammonium $[(iBu)_2NPrH]^+$, an assignment consistent with the MS^2 spectrum which shows the elimination of C_4H_8 to form *m/z* 116. *M/z* 130 is the dibutyl ammonium cation $[(iBu)_2NH_2]^+$; these two amines have been observed in previous studies of CMPO degradation by direct infusion ESI.

The samples from the highest dose experiments (TOS 7, 8 and 9) contained abundant ions from DBP, which arises from radiolysis of TBP. The DBP conjugate base at *m/z* 211 is accompanied by fragment ions at *m/z* 155 and 99; in addition there are cluster ion series at *m/z* 421, 631, and 841 that correspond to $[(DBP)_{2\text{-}4}H]^+$, and 443, 653, and 883 that correspond to $[(DBP)_{2\text{-}4}Na]^+$. The two protonated amine degradation products at *m/z* 130 and *m/z* 172 are present in abundance, as are unidentified product ions at *m/z* 260 and 118. Ions derived from intact lactic acid, DTPA, and CMPO are in very low abundance in the spectra of the high dose samples, indicating that they have undergone nearly complete radiolytic degradation.

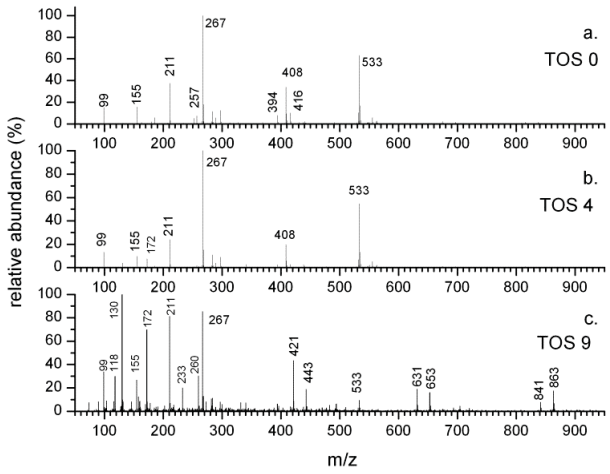

Figure A-9. Positive ESI mass spectra of TOS samples 0, 4 and 9.

Trends in ion abundance with increasing sample number (radiation dose) are more easily seen in the positive ion infusion profiles (see Figure A-10). The DTPA-derived ions (sum of the *m/z* 394 and 416 intensities) undergo a steady decrease with increasing dose. In the unirradiated TOS 0, the intensities of the DTPA lactam ions is negligible, but these ions increase in the spectrum of the lowest dose sample TSO 4, and then decrease at higher dose. This indicates that the lactam undergoes subsequent degradation, however exactly what it turns into hasn't been identified.

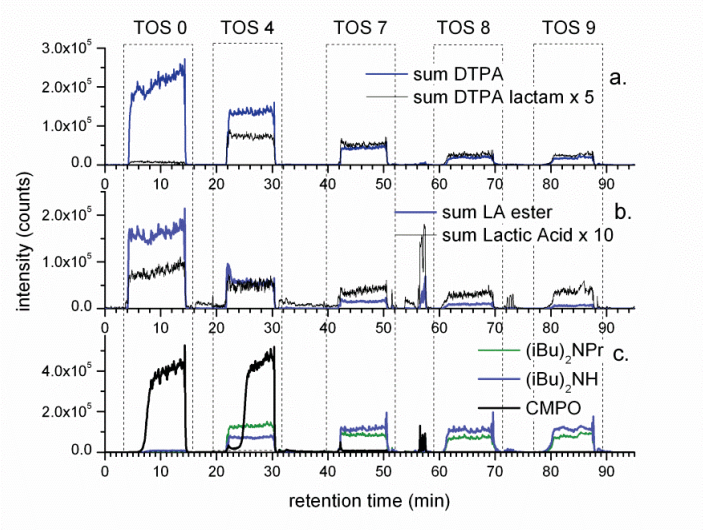

Figure A-10. Positive ion infusion profiles for the TOS samples. The DTPA ions are *m/z* 394 and 416. DTPA lactam ions are *m/z* 318 and 340. The lactic acid ions are *m/z*91, 113, and 135. The LA-ester ions are *m/z* 163, 185 and 257. CMPO is *m/z* 408. (iBu)2NPr is *m/z* 172, and (iBu)2NH is *m/z* 130.

The intensities of the lactic acid ions $[(LA)H]^+$, $[(LA)Na]^+$ and $[(LA\text{-}H)Na_2]^+$ are very low thoughout the set of positive ion analyses, and they decrease with increasing dose. The intensities of the ions derived from the esterified lactic acid (*m/z* 163, 185, and 257) are reasonably large in the TOS 0 sample, and they also drops rapidly with increasing dose. This indicates that the esters are present in the unirradiated sample, and that they are very sensitive to irradiation. We hypothesize that the esters are formed in the DTPA-containing aqueous layer, since direct infusion analyses of a 6 mM sodium lactate solution contained only ions derived from sodium lactate (data not shown), and did not contain any ions derived from the esters.

An abundant CMPO ion at *m/z* 408 is observed in the TOS 0 sample, and corresponds to $[(CMPO)H]^+$. The intensity of this ion stays relatively abundant in the TOS 4 irradiated sample, but is practically gone by TOS 7. The fact that the intensity of $[(CMPO)H]^+$ did not decrease in the TOS 4 sample was surprising; however we believe that the decrease in its intensity due to radiolysis is offset by an increase in entrainment of the organic compounds that occurs when radiation is initiated (as noted below for TBP). The CMPO degradation products diisobutyl amine and diisobutyl,propyl amine are seen as protonated ions at *m/z* 130 and 172. They have been observed in previous direct infusion studies of radiolyzed CMPO, and their abundances persist at relatively high levels in the samples receiving the higher radiation doses. CMPO is also observed in the expanded mass spectrum of sample T3, showing up as the protonated molecule at *m/z* 408. In addition, ions at *m/z* 130 and 297 are observed, which have been shown in prior studies to be derived from CMPO radiolysis products, the former diisobutyl amine, and the latter the CMPO carboxylic acid (see Figure A-11).

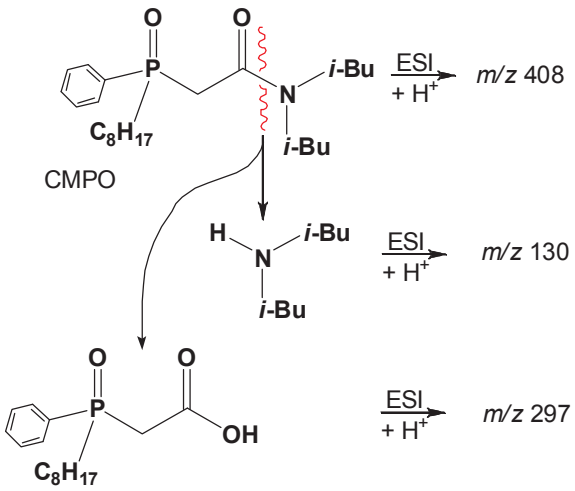

Figure A-11. Radiolysis reactions of CMPO producing degradation products responsible for *m/z* 130 and 297.

TBP displays surprising behavior in that the intensities of $[(TBP)H]^+$ and $[(TBP)_2H]^+$ at *m/z* 267 and 533 initially increase when irradiation is initiated (comparing TOS 0 to TOS 4, data not shown), but then decreases in a precipitous fashion in the samples receiving higher doses. We hypothesize that initial irradiation makes the aqueous samples better able to entrain TBP, probably resulting from the formation of smaller more hydrophilic organic compounds.

The numerical average intensities for the positive ions resulting from lactic acid, DTPA, and degradation products formed in the static irradiation of the TRUEX strip aqueous phase in contact with TRUEX solvent are summarized in Table A-7.

Table A-7. Averaged absolute intensities of the LA, DTPA and CMPO -derived cations in the analyses of the TOS samples.

Absorbed Dose, kGy	LA+H	LA+Na	LA-H+2Na	sum DTPA lactam	DTPA lactam+H	DTPA lactam+Na
	m/z 91	*m/z* 113	*m/z* 135		*m/z* 318	*m/z* 340
0.0	2559	1957	7755	577	287	290
342	1238	1628	989	14494	7958	6536
972	1383	1007	559	10830	5271	5559
1130	499	773	334	5543	2421	3122
1320	489	1063	373	4575	2008	2567

Table A-7 (con't). Averaged absolute intensities of the LA, DTPA and CMPO -derived cations in the analyses of the TOS samples.

Absorbed Dose, kGy	sum DTPA	DTPA-H	DTPA-2H+Na	CMPO	(iBu)2NPr	(iBu)2NH
		m/z 394	*m/z* 416	*m/z* 408	*m/z* 172	*m/z* 130
0.0	207086	90957	116129	394487	1965	7755
342	86878	42121	44757	350139	128738	70064
972	32895	19929	12966	7516	86984	113813
1130	15052	7793	7259	474	71311	106772
1320	11421	6945	4476	556	113059	78826

Negative ion direct infusion studies

The anion mass spectrum of the TOS 0 sample (no dose) had a base peak at *m/z* 89 corresponding to $[LA-H]^-$, an ion at *m/z* 161 that is derived from the conjugate base of the lactate self-ester (see Figure A-12). Ions at *m/z* 392 and 414 are the DTPA conjugate base, and the mono-natiated derivative.

Irradiation causes a decrease in the abundance of both lactic acid and DTPA, as seen in the spectrum of sample TOS 4. This is observed on both a relative basis and on an absolute basis. The base peak in the spectrum for TOS 4 is *m/z* 209, which is the DBP conjugate base. A lower abundance *m/z* 153 is a DBP fragment ion. A relatively prominent ion at *m/z* 177 is thought to be a cluster formed from lactic acid and pyruvic acid, which we hypothesize to be a radiolysis product of lactic acid. The conjugate base of pyruvic acid at *m/z* 87 is very low abundance, which may reflect its ability to make cluster ions in ESI.

In the spectra of the samples TOS 7, 8, and 9 (subjected to higher doses) DTPA is for the most part absent from the spectrum, and the abundance of lactic acid- and lactic acid ester-derived ions are much reduced in intensity. This suggests that all three compounds are degraded by the application of radiation dose. In contrast, the absolute intensities of the DBP-related ions continues to increase with increasing dose.

Trends in absolute ion abundance are more apparent in the infusion profiles, which show changes in the intensities of individual ions as the sample is switched (and radiation dose is increased, see Figure A-13). The lactic acid conjugate base $[LA-H]^-$ at *m/z* 89 decreases with dose to sample TOS 8, but holds constant after that at about 40% of its initial intensity. Pyruvate and the putative pyruvate-lactate cluster

at *m/z* 87 and 177 respectively do the inverse, rising from low abundance in the spectrum of TOS 0, achieving relatively equivalent intensities in samples TOS 4, ,7, 8, and 9. The LA ester signal at *m/z* 161 undergoes fairly rapid degradation, indicating that it is present at the beginning of the experiments, but is fairly sensitive to radiolysis reactions.

The numerical average intensities for the positive ions resulting from lactic acid, DTPA, and degradation products formed in the static irradiation of the TRUEX strip aqueous phase in contact with TRUEX solvent are summarized in Table A-8.

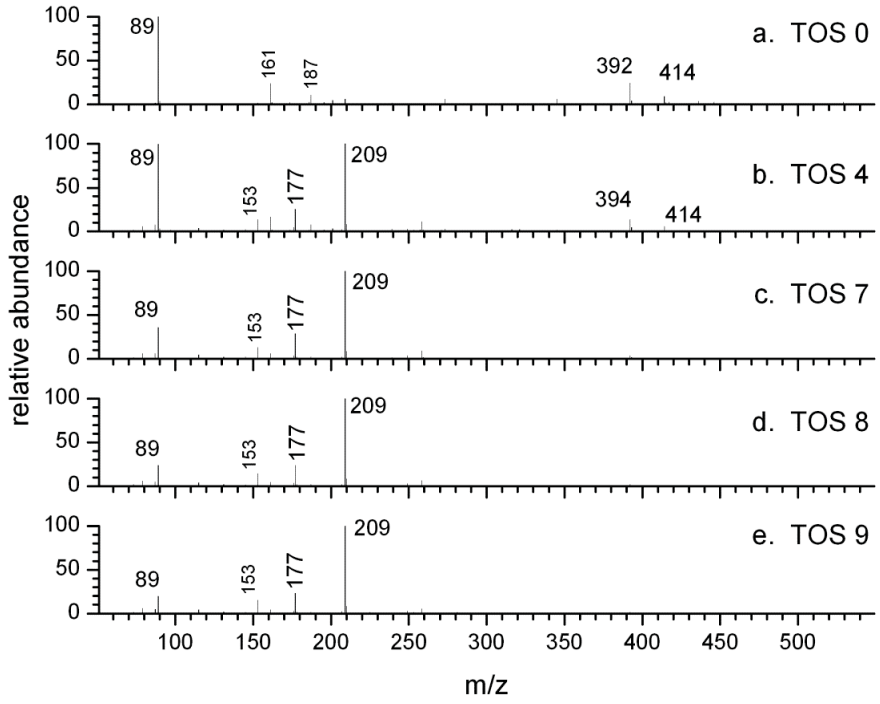

Figure A-12. Negative ESI mass spectra of the TOS series samples.

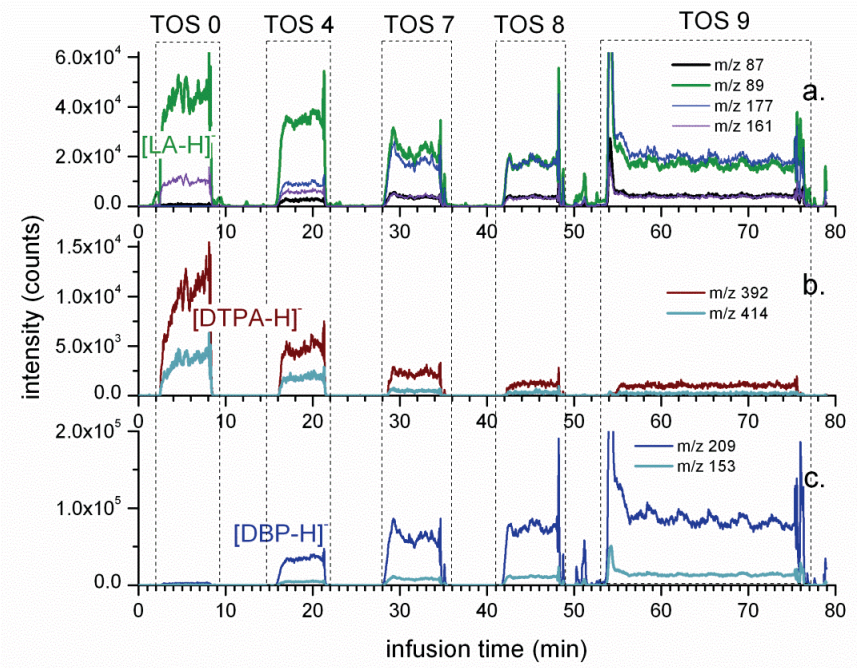

Figure A-13. Negative ion infusion profiles for the TOS samples. The DTPA ions are *m/z* 392 and 414. DBP ions are *m/z* 209 and 153. Lactic acid is *m/z* 89, pyruvic acid *m/z* 87, and the LA ester *m/z* 161.

Table A-8. Averaged absolute intensities of the LA, DTPA and CMPO-derived anions in the analyses of the TOS samples.

Absorbed Dose, kGy	Pyr-H	LA-H	LA ester-H	DBP-H	sum DTPA	DTPA-H	DTPA-2H+Na
	m/z 87	*m/z* 89	*m/z* 161	*m/z* 209		*m/z* 392	*m/z* 414
0.0	676	44362	10360	2471	14526	10699	3827
0.0	2643	35309	5924	35427	6715	4849	1866
342	3715	21818	3802	61153	2698	2250	448
972	3680	17592	3367	74613	1528	1206	322
1130	4078	17131	3719	87711	1190	960	230

Analysis of Test Loop Samples, T Series.

Test Loop Samples, Positive Ion Analyses.

The positive ion analysis of the T0 sample displayed intense ions derived from the lactate esters and DTPA. DTPA furnished a protonated molecular ion $[(DTPA)H]^+$ at *m/z* 394, which was accompanied by natiated ions at *m/z* 416 and 438 (see Figure A-14, Table A-9). The relatively high intensity of these ions was consistent with their relatively high concentration in the spray solution. The other dominant ions in the T0 positive ion spectra are derived from lactate self esterification having molecular weights of 162 (monoester) and 234 (diester) g/mol. These esters are present in the stock lactic acid used to make the aqueous phase, and are the result of lactic acid self-esterification. The esters are efficiently recorded in the positive ion spectrum as either protonated, ammoniated or natiated species at *m/z* 163, 180, 185, 235, 252 and 257, respectively. There are also clusters with lactic acid at *m/z* 347 and 369. Lactic acid itself did not strongly register as an intact species in these experiments; a low intensity ion is seen at *m/z* 91, but it is not in accord with the concentration of lactate in the ESI spray solutions (6 mM).

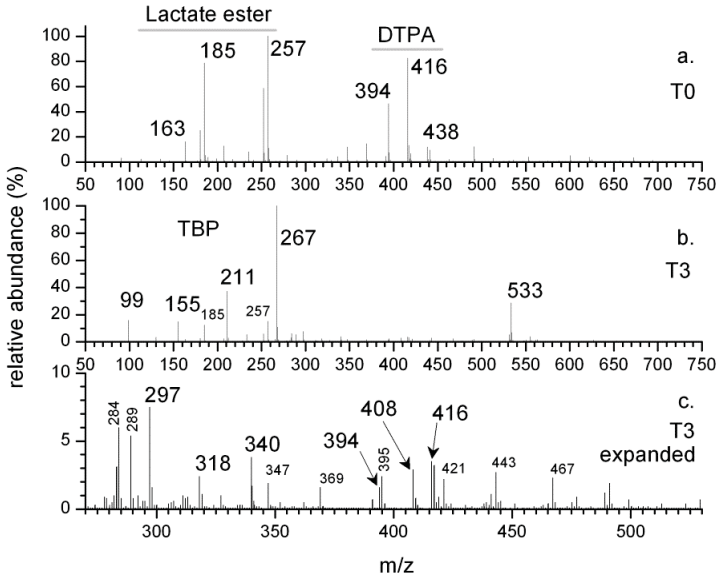

Figure A-14. Positive ESI mass spectra comparing test loop samples T0 and T3.

Table A-9. Ion compositions corresponding to ions seen in the positive ion mass spectra of the test loop samples.

m/z	Composition	Compound derived from	Absorbed Dose, kGy
653	$[(DBP)_3Na]^+$	HDBP	1270
631	$[(DBP)_3H]^+$	HDBP	1270
533	$[(TBP)_2H]^+$	TBP	405
467	$[(DBP\text{-}H)(DBP)H]^+$	HDBP	405
443	$[(DBP)_2Na]^+$	HDBP	1270
438	$[(DBP)_2NH_4]^+$	HDBP	1270
438	$[(DTPA\text{-}H)Na_2]^+$	DTPA	0.0
421	$[(DBP)_2H]^+$	HDBP	1270
417	$[(LA\ ester)(DBP)Na]^+$	HDBP, LA	405
416	$[(DTPA)Na]^+$	DTPA	0.0
408	$[(CMPO)H]^+$	CMPO	405
395	$[(LA\ ester)(DBP)H]^+$	HDBP, LA	405
394	$[(DTPA)H]^+$	DTPA	0.0
369	$[(LA\ diester)(LA)Na]^+$	LA	405
347	$[(LA\ diester)(LA)H]^+$	LA	405

340	$[(\text{DTPA lactam})\text{Na}]^+$	DTPA	405
318	$[(\text{DTPA lactam})\text{H}]^+$	DTPA	405
297	$[(\text{CMPO acid})\text{H}]^+$	CMPO	405
289	$[(\text{TBP})\text{Na}]^+$	TBP	405
284	$[(\text{TBP})\text{NH}_4]^+$	TBP	405
267	$[(\text{TBP})\text{H}]^+$	TBP	405
257	$[(\text{LA diester})\text{Na}]^+$	LA	0.0
252	$[(\text{LA diester})\text{NH}_4]^+$	LA	0.0, 405
211	$[(\text{DBP})\text{H}]^+$	HDBP, TBP	405, 1270
185	$[(\text{LA ester})\text{Na}]^+$	LA	0.0, 405
180	$[(\text{LA ester})\text{NH}_4]^+$	LA	0.0, 405
163	$[(\text{LA ester})\text{H}]^+$	LA	0.0, 405
155	$[(\text{MBP})\text{H}]^+$	HDBP, TBP	405, 1270
99	$[(\text{H}_3\text{PO}_4)\text{H}]^+$	HDBP, TBP	405, 1270

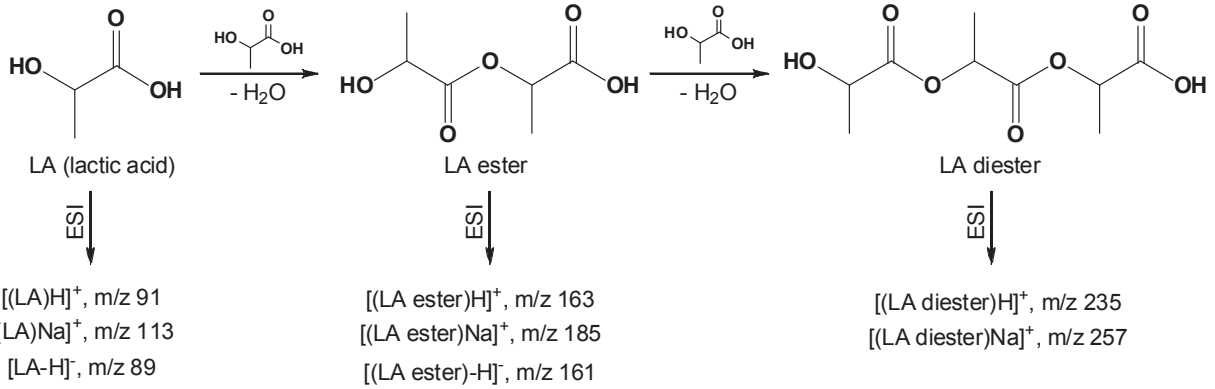

Figure A-14. Lactate self esterification reactions producing ions seen in T0.

The positive ion analysis of the T3 sample contained abundant signal derived from TBP, which shows up as the protonated molecule at *m/z* 267 $[(TBP)H]^+$. Under ESI conditions, $[(TBP)H]^+$ undergoes elimination of 1, 2, and 3 C_4H_8 molecules forming *m/z* 211, 155 and 99, respectively. In addition, TBP in the test loop undergoes elimination of C_4H_8, forming HDBP and H_2MBP, and these also produce ion signals at *m/z* 211, 155 and 99. At higher radiation doses, these ion signals are augmented, while that of intact TBP is less intense, signalling clearly that TBP radiolysis is occurring. In sample T3, there is no doubt that some of the signal at *m/z* 211, 155 and 99 is derived from radiolytic TBP-derived products, however some of the signal at at these *m/z* values are also the result of ionic fragmentation reactions.

The very high abundance of TBP-derived ions, and the lack of intense LA- or DTPA-derived ions is a consequence of a couple of factors, the first of which is the high sensitivity of ESI for TBP. TBP is a highly nucleophilic molecule as a result of its very high dipole moment, and at the same time is very surfacting, an attribute derived from its three hydrophobic butyl groups. This type of molecule will occupy surface sites on the ESI droplets, a location that favors ion formation. Still, its presence in the aqueous phase was surprising. We believe that radiolytic changes to the LA – DTPA system have produced compounds that favor entrainment of some TBP in the aqueous phases. This may be due to the fact that DTPA has degraded to some degree. An expansion of the T3 mass spectrum from *m/z* 270 – 530 shows that the signature ions for intact DTPA are still present at *m/z* 394 and 416 (see Figure A-15c), but at much lower intensity compared to the spectrum of the T0 sample. Two new ions are observed at *m/z* 318 and 340 that are unequivocally derived from DTPA degradation; this conclusion is supported by accurate *m/z* measurements, which are consistent with the proposed elemental composition (see below), and by collision induced dissociation (CID) reactions. The fact that the two ions are separated by 22 u indicates that *m/z* 318 is protonated, while *m/z* 340 is natiated. Thus the molecular weight of the degradation product is 317 g/mol, representing a loss of 76 g/mol compared to DTPA. There are other ions observed in the expanded mass spectrum of sample T3, however these can nearly all be explained as cluster ions formed from combinations of the lactate esters, lactic acid, and HDBP (see Table A-9).

The mass spectrum of the T5 sample (Figure A-15a) was very similar to that of T3; it is certain that radiolysis is proceeding, however the spectral similarity is probably due to the strong influence of TBP on the analysis. Changes in the spectrum of T6 are observed, namely that the DBP-derived ions at *m/z* 211, 155 and 99 are more abundant, and DBP cluster ions are now observed at *m/z* 421 and 443 that correspond to $[(DBP)_2H]^+$ and $[(DBP)_2Na]^+$. The final sample in the series is T7, which received the highest dose. TBP is still observed at *m/z* 267 albeit at lower abundance, indicating that radiolysis has degraded most of this compound. Instead, the spectrum is dominated by DBP-derived ions mentioned above, and in addition, higher DBP cluster ions are observed at *m/z* 631, 653, 841 and 863. There is no

longer any indication of intact DTPA, however the DTPA lactam derived ions at *m/z* 318 and 340 can still be seen. It is certain that the DTPA lactam is undergoing further degradation however additional products cannot be assigned as yet.

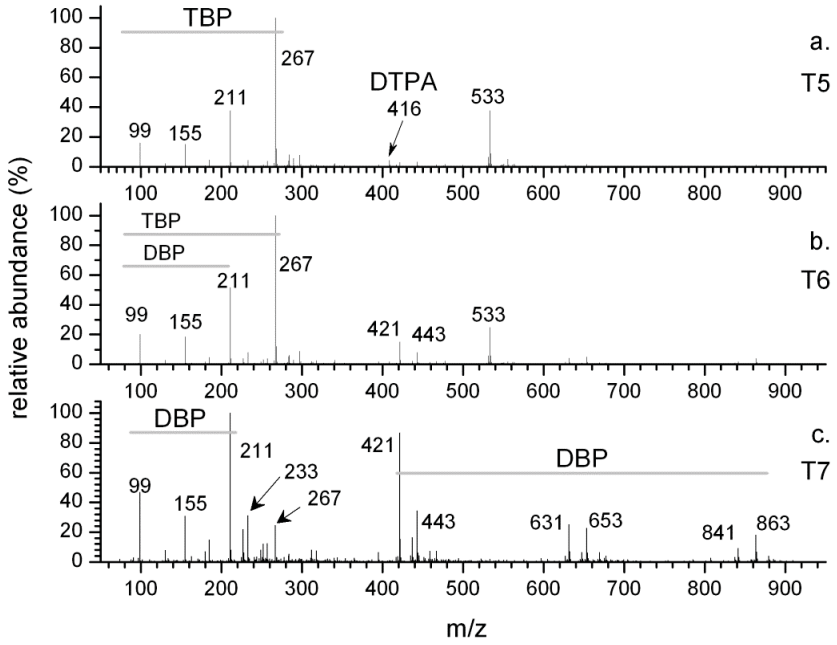

Figure A-15. Cation ESI mass spectra of samples T5, T6 and T7.

A semiquantitative view of the radiolysis behavior can be gained by plotting the infusion profiles of ion intensities as the sample is changed from T0 to T7 (i.e., dose is increased, Figure A-16). The intensities of the sum of the DTPA-derived ions (*m/z* 394, 416, 438) decreased by a factor of about 6 on going from sample T0 to T3, and continued to decrease steadily after that. The DTPA lactam profiles (sum of *m/z* 318 and 340) increased dramatically on going from T0 to T3, but then decrease in sample T7, indicating radiolysis of the lactam. Ions derived from LA display only modest decreases however the LA-ester derivatives decrease very dramatically. The infusion profiles of the TBP derived ions (*m/z* 267 and 533) increase from effectively zero in T0 to 1 x 10^6 counts in T3, continue to increase in T5, but then fall dramatically. The HDBP derived ions (*m/z* 211, 155, 99 and the cluster ions at 421, 443, 631, 653, 841 and 863) also increase on going from T0 to T3, but in contrast to TBP they climb in intensity, indicating that they are being formed by radiolysis. The behavior of CMPO is similar to that of TBP, indicating that radiolysis initially helps to entrain CMPO, but later on causes it to degrade.

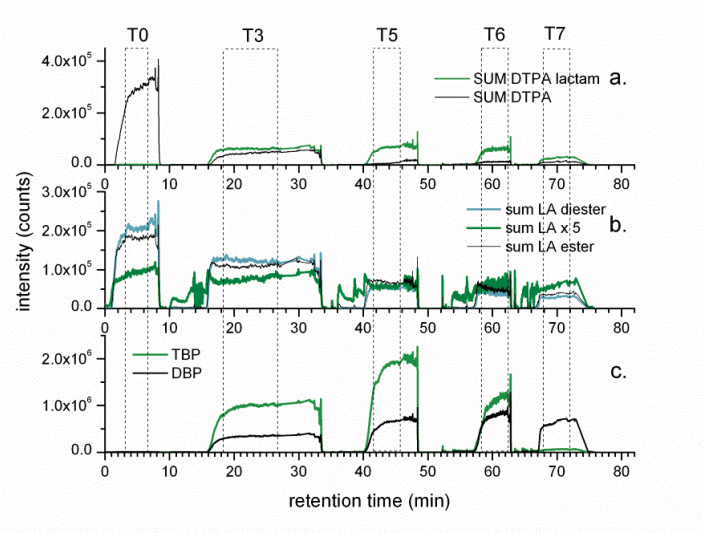

Figure A-16. Infusion profiles, test loop samples T0, T3, T5, T6 and T7. Top, DTPA-derived. Bottom, DTPA lactam derived.

Numerically averaged ion intensities are provided in Table A-10.

Table A-10. Numerical averages for the important cations derived from LA, LA esters, DTPA, TBP and CMPO in the T series of samples (Test Loop).

Sample	Absorbed Dose, kGy	*m/z* 394	*m/z* 438	*m/z* 416	sum DTPA
TS0	0.0	86900	22589	155708	265197
TS3	405	12145	3352	26471	41968
TS5	733	594	2749	541	3884
TS6	1043	679	1052	608	2339
TS7	1270	577	5088	650	6315

Table A-10 (con't). Numerical averages for the important cations derived from LA, LA esters, DTPA, TBP and CMPO in the T series of samples (Test Loop).

Sample	Absorbed Dose, kGy	*m/z* 318	*m/z* 340	sum DTPA lactam
TS0	0.0	240	311	551
TS3	405	18488	28965	47453
TS5	733	17092	20244	37336
TS6	1043	21471	22828	44299
TS7	1270	14514	5073	19587

Table A-10 (con't). Numerical averages for the important cations derived from LA, LA esters, DTPA, TBP and CMPO in the T series of samples (Test Loop).

Sample	Absorbed Dose, kGy	*m/z* 91	*m/z* 113	*m/z* 135	sum LA
TS0	0.0	5914	4404	4587	14905
TS3	405	5034	4035	3076	12145
TS5	733	2970	3237	2402	8609
TS6	1043	5023	2283	2420	9726
TS7	1270	5511	1334	2445	9290

Table A-10 (con't). Numerical averages for the important cations derived from LA, LA esters, DTPA, TBP and CMPO in the T series of samples (Test Loop).

Sample	Absorbed Dose, kGy	*m/z* 163	*m/z* 185	sum LA ester	*m/z* 235	*m/z* 257	sum LA diester
TS0	0.0	30630	147698	178328	15235	187699	202934
TS3	405	13659	94515	108174	42465	115952	158417
TS5	733	5998	59540	65538	2958	48431	51389
TS6	1043	7749	39848	47597	4090	33358	37448
TS7	1270	7245	28476	35721	3827	23695	27522

Table A-10 (con't). Numerical averages for the important cations derived from LA, LA esters, DTPA, TBP and CMPO in the T series of samples (Test Loop).

Sample	Absorbed Dose, kGy	*m/z* 267	*m/z* 533	sum TBP	*m/z* 408	*m/z* 430	sum CMPO
TS0	0.0	231	0	231		27	27
TS3	405	834679	223024	1.0577E6	66619	5527	72146
TS5	733	1.41278E6	521618	1.9344E6	160738	11285	172023
TS6	1043	923670	241218	1.16489E6	21893	1191	23084
TS7	1270	27893	936	28829	3106	621	3727

Test Loop Samples, Negative Ion Analyses.

The anion analysis of test loop sample T0 showed an abundant ion at *m/z* 89 that corresponds to the lactic acid conjugate base $[LA\text{-}H]^-$ (Figure A-17). Other ions in the spectrum correspond to the lactic acid self esterification reaction, or clusters of this and lactic acid (Table A-11). The exception to this is *m/z* 187, which has not been satisfactorily identified, however it eliminates $C_3H_4O_2$ (72 amu) which is a signature for compounds esterified with lactic acid. In addition to products derived from lactate, ions derived from DTPA were in abundance in the T0 analysis, highlighted by the conjugate base at *m/z* 392. In addition natiated versions were seen at *m/z* 414 and 436, which are formed by Na-for-H substitution in the ESI droplets. These ions confirm the DTPA assignments made for the T0 positive ion analysis, being 2 amu lower (two protons, switching the polarity from positive to negative).

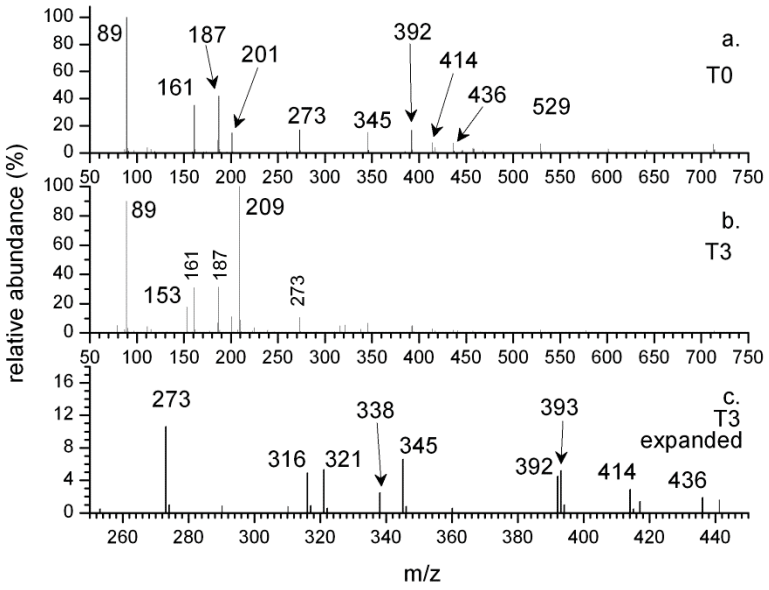

Figure A-17. Anion ESI spectra of test loop samples T0 and T3.

Table A-11. Compositions and origins of anions seen in the ESI mass spectra of the test loop samples.

m/z	Composition	Compound derived from	Absorbed Dose, kGy
436	$[(DTPA\text{-}H)Na_2]^-$	DTPA	0.0
414	$[(DTPA)Na]^-$	DTPA	0.0
393	$[(DBP\text{-}H)(LA\text{-}ester\text{-}H)Na]^-$	HDBP, LA	405
392	$[DTPA\text{-}H]^-$	DTPA	405
345	$[(LA\text{-}ester\text{-}H)_2Na]^-$	LA	0.0
338	$[(DTPA\ lactam\text{-}2H)Na]^-$	DTPA	405
321	$[(DBP\text{-}H)(LA\text{-}H)Na]^-$	HDBP, LA	405
316	$[DTPA\ lactam\text{-}H]^-$	DTPA	405
273	$[(LA\text{-}ester\text{-}H)(LA\text{-}H)Na]^-$	LA	0.0
209	$[DBP\text{-}H]^-$	HDBP	405
201	$[(LA\text{-}H)_2Na]^-$	LA	0.0
161	$[LA\text{-}ester\text{-}H]^-$	LA	0.0
89	$[LA\text{-}H]^-$	LA	0.0

The anion ESI mass spectrum of T3 contained abundant ions derived from HDBP, notably the conjugate base at *m/z* 209, and cluster ions with lactate and the lactate ester at *m/z* 321 and 393 (Figure A-18Figure b,c). The ion at *m/z* 153 is likely derived from both HDBP (as a fragmentation product of the conjugate base at *m/z* 209) and from conjugate base of monobutylphosphoric acid H_2MBP. The DTPA signature ions at *m/z* 392 and 414 are still seen, albeit at lower abundance, and the DTPA lactam conjugate base is now observed at *m/z* 316, together with the natiated ion at *m/z* 338. These ions are

complementary to the cations seen for this compound at *m/z* 318 and 340, and further confirm the existence of a degradation product having a molecular weight of 317 g/mol, that we hypothesize to be the DTPA lactam.

The anion spectra of samples T5, T6 and T7 are very similar, containing the same ions noted above for sample T3, with the salient exception that the DTPA conjugate base is gone (see Figure A-18). This no doubt signals complete radiolysis of DTPA by the dose corresponding to T5. The ions derived from the DTPA lactam at *m/z* 316 and 338 are still present, although they appear decreased in abundance compared to sample T3; this suggests that the lactam undergoes radiolysis, however we have not yet determined what it becomes.

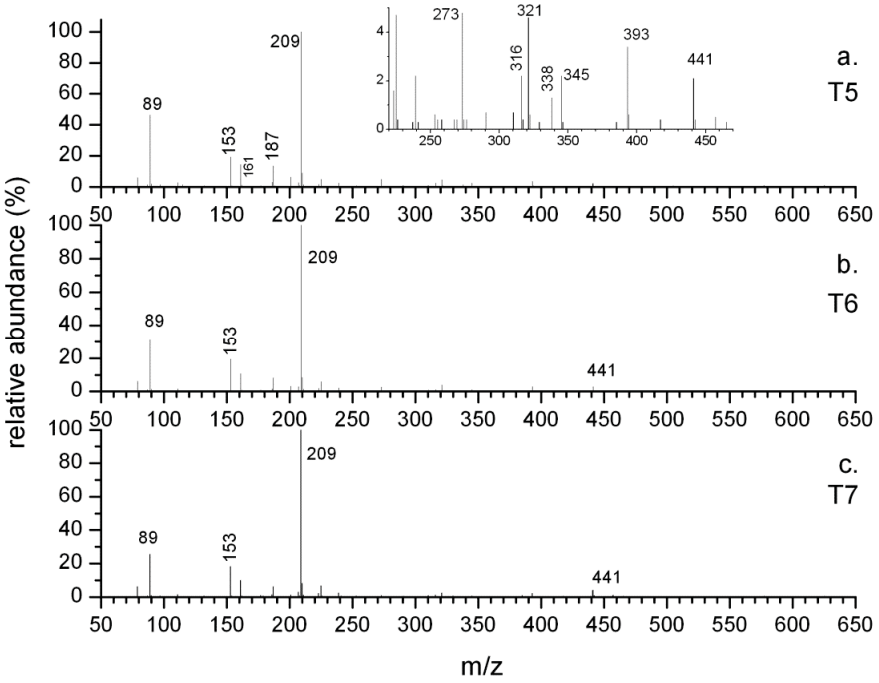

Figure A-18. Anion ESI-mass spectra of samples T5, T6 and T7. The inset in a is an expanded view (20X) from *m/z* 220 to 470.

Temporal profiles are shown in Figure A-19; DTPA decreases to almost zero by T5, as the lactam increases. At higher doses, the lactam also decreases. Lactate and the ester also decrease, but remain measurable at the highest doses. DBP and *m/z* 153 progressively increase as dose increases. *m/z* 153 can arise by ion fragmentation of $[DBP\text{-}H]^-$ and as the conjugate base of H_2MBP.

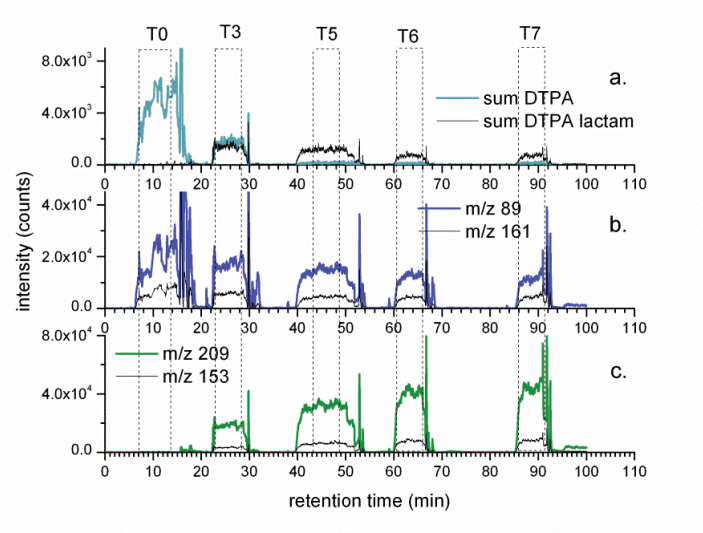

Figure A-19. Infusion profiles for anions derived from DTPA, DTPA lactam, lactate (89), lactate ester (161), DBP (209), and MBP (153), T series (Test Loop) analyses.

Averaged ion intensities are provided for the anion analyses of the test loop (T series) samples in Table A-12.

Table A-12. Numerical averages for the important anions derived from LA, LA esters, DTPA, TBP and CMPO in the T series of samples (Test Loop).

Absorbed Dose, kGy	*m/z* 392	*m/z* 414	*m/z* 436	sum DTPA	*m/z* 316	*m/z* 338	sum DTPA lactam
	DTPA+H	DTPA+Na	DTPA-H+Na2		DTPA lactam + H	DTPA lactam + Na	
0.0	2281	1025	981	4287	12	6	18
405	831	534	355	1720	907	461	1368
733	47	20	37	104	715	404	1119
1043	17	3	13	33	454	200	654
1270	19	17	22	58	512	148	660

Table A-12. Numerical averages for the important anions derived from LA, LA esters, DTPA, TBP and CMPO in the T series of samples (Test Loop).

Absorbed Dose, kGy	*m/z* 87	*m/z* 89	*m/z* 161	*m/z* 153	*m/z* 209
	pyruvate	lactate	lactate ester	H_2MBP	HDBP
0.0	346	13648	4811	0	56
405	438	16610	5732	3270	18471
733	432	14933	4540	6184	32294
1043	404	12975	4416	8034	41654
1270	339	11255	4419	8076	43898